nature plants

ARTICLES

https://doi.org/10.1038/s41477-021-00862-9

GDSL-domain proteins have key roles in suberin polymerization and degradation

Robertas Ursache[1]✉, Cristovão De Jesus Vieira Teixeira[2], Valérie Dénervaud Tendon[1], Kay Gully[1], Damien De Bellis[1,3], Emanuel Schmid-Siegert[4,7], Tonni Grube Andersen[1,8], Vinay Shekhar[2,5], Sandra Calderon[4,6], Sylvain Pradervand[4,6], Christiane Nawrath[1], Niko Geldner[1]✉ and Joop E. M. Vermeer[2,5]✉

Plant roots acquire nutrients and water while managing interactions with the soil microbiota. The root endodermis provides an extracellular diffusion barrier through a network of lignified cell walls called Casparian strips, supported by subsequent formation of suberin lamellae. Whereas lignification is thought to be irreversible, suberin lamellae display plasticity, which is crucial for root adaptative responses. Although suberin is a major plant polymer, fundamental aspects of its biosynthesis and turnover have remained obscure. Plants shape their root system via lateral root formation, an auxin-induced process requiring local breaking and re-sealing of endodermal lignin and suberin barriers. Here, we show that differentiated endodermal cells have a specific, auxin-mediated transcriptional response dominated by cell wall remodelling genes. We identified two sets of auxin-regulated GDSL lipases. One is required for suberin synthesis, while the other can drive suberin degradation. These enzymes have key roles in suberization, driving root suberin plasticity.

Plants require a dynamic and adaptive root system, which enables optimal anchorage and foraging of the soil environment for water and nutrients, while managing interactions with the soil microbiome[1–3]. Lateral root formation is a key factor modulating root system architecture. In most angiosperms, including *Arabidopsis thaliana*, these organs initiate in xylem-pole associated pericycle cells (XPPs). Auxin is required for both initiation and development of lateral roots[4,5]. Lateral roots need to traverse the overlying endodermis to develop and emerge, and this cell layer therefore has an essential role during lateral root formation, as it has to actively accommodate the expansion growth of the XPPs through remodelling of cell shape and volume.

Moreover, to minimize both the leakage of nutrients from the stele into the rhizosphere and the entry of soil-borne pathogens, opening and sealing of the lignified and suberized endodermal barriers needs to be tightly controlled. Therefore, a dynamic desuberization and resuberization is bound to have an important role in this process. However, we still lack an understanding of the basic molecular machineries that regulate the dynamics of suberin deposition and degradation during root development[6–9]. The lignified Casparian strip appears to be locally modified to allow the growth of the lateral root through this cell layer[10] and it suberin has been shown to be deposited in the cell walls of endodermal cells in contact with the later lateral root primordium after emergence[8]. However, endodermal cells are often already suberized when lateral roots form and it is unknown how suberin is first degraded and later resynthesized.

All these responses are regulated via auxin-mediated signalling in the endodermis, and expression of *short hypocotyl 2-2* (*shy2-2*)—a dominant repressor of auxin signalling—in this cell layer blocks lateral root formation, demonstrating the crucial role of SHY2-mediated endodermal auxin signalling in this process[10].

In this Article, we show that differentiated endodermal cells have a distinct auxin-mediated transcriptome. We analysed this dataset and identified a set of ten GDSL-motif-containing enzymes that are differentially regulated after auxin treatment. We confirmed that all ten of these GDSL-motif-containing enzymes were expressed in the endodermis, and were either repressed or induced during auxin treatment or lateral root formation. We showed that five of the auxin-repressed GDSL-motif-containing enzymes are redundantly required for suberin biosynthesis; the quintuple knockout of these enzymes essentially abrogated suberin accumulation in the endodermis. Among the five auxin-induced GDSL-motif-containing genes, we identified enzymes that we demonstrated to be sufficient for suberin degradation and required for correct lateral root emergence. The quintuple mutants of the suberin-biosynthetic, GDSL-motif-containing enzymes were highly sensitive to mild salt stress. Single-knockout mutants of members of the suberin-degrading class displayed delays in lateral root emergence. The enzymes identified in this work are strong candidates to be suberin polymerases and degradases in plants. This work advances our understanding of in vivo suberin formation, as well as the mechanisms underlying its developmental plasticity.

Results

A genotype for obtaining specific endodermal auxin responses. Drastic changes in endodermal cell volume and Casparian strip modification during lateral root emergence[10] are mediated by

[1]Department of Plant Molecular Biology, University of Lausanne, Lausanne, Switzerland. [2]Laboratory of Cell and Molecular Biology, Institute of Biology, University of Neuchâtel, Neuchâtel, Switzerland. [3]Electron Microscopy Facility, University of Lausanne, Lausanne, Switzerland. [4]Vital-IT Competence Center, Swiss Institute of Bioinformatics, Lausanne, Switzerland. [5]Department of Plant and Microbial Biology & Zurich–Basel Plant Science Centre, University of Zurich, Zurich, Switzerland. [6]Genomic Technologies Facility, University of Lausanne, Lausanne, Switzerland. [7]Present address: NGSAI, Epalinges, Switzerland. [8]Present address: Max Planck Institute for Plant Breeding Research, Cologne, Germany. ✉e-mail: Robertas.Ursache@unil.ch; Niko.Geldner@unil.ch; Josephus.Vermeer@unine.ch

SHORT HYPOCOTYL 2 (*SHY2* (also known as *IAA3*))-dependent auxin signalling. SHY2 represses its own transcription in a typical, auxin-induced negative-feedback loop and is thus also an early transcriptional auxin-response marker in the endodermis[10,11]. The targets of SHY2 (direct or indirect) that drive the complex accommodating responses in the endodermis remain unknown. Therefore, we set out to obtain a SHY2-mediated transcriptional response profile in the endodermis. Generating such a dataset comes with particular challenges. First, most endodermal cells at the moment of lateral root emergence are lignified and suberized, making it impossible to use protoplast isolation for single-cell or cell-type-specific sequencing. Second, only a subset of endodermal cells—those overlying an auxin-emitting lateral root primordium from stage I and onwards—will be stimulated in a *SHY2*-dependent fashion[10]. We therefore first compared wild-type and *CASP1pro::shy2-2* seedlings—in which auxin signalling is suppressed specifically in the differentiated endodermis—after auxin treatment to obtain an endodermis-specific set of auxin-responsive genes. In the wild type, the auxin-reporter *SHY2pro::NLS-3xmVenus* fluorescence peaks in the endodermis at about 16 h after treatment with the membrane-permeable auxin analogue NAA and is blocked in the *CASP1pro::shy2-2* line (Fig. 1a,d and Extended Data Fig. 1). However, since the *CASP1pro::shy2-2* transgene also indirectly impairs the auxin-mediated induction of lateral roots[10], a simple comparison of the auxin-induced transcriptomes of *CASP1pro::shy2-2* roots and wild-type roots after auxin treatment would be dominated by pericycle and cell cycle-related responses, preventing identification of endodermal auxin responses. Therefore, we added a genetic manipulation that would strongly enrich for auxin-induced transcriptional changes in the endodermis. We combined the dominant *solitary root 1* (*slr-1* (also known as *iaa14*)) mutant with *CASP1pro::shy2-2*. Lateral root formation is impaired in the *Arabidopsis slr-1* mutant[12]. Importantly, *SLR* is expressed in the pericycle, cortex and epidermis, but not in the endodermis, and the *slr-1* mutant should thus specifically block auxin response in the cell layers surrounding the endodermis[12,13](Extended Data Fig. 2a). As predicted, we found that auxin-mediated induction of *SHY2* in the endodermis still occurred in *slr-1* roots (Fig. 1b,d). We further predicted that, in the combined *CASP1pro::shy2-2/slr-1* background, auxin signalling should be largely blocked in all differentiated root cell layers. Indeed, we could not detect induction of *SHY2pro::NLS-3xmVenus* in the endodermis in this background. Based on these results, we predicted that a comparison (subtraction) of the NAA-induced transcriptomes of roots from the *slr-1* single mutant with the *CASP1pro::shy2-2/slr-1* double mutant would enable us to extract a specific endodermal auxin signalling transcriptomic profile, which would otherwise be obscured by the strong, proliferation-inducing auxin responses of the XPPs (Fig. 1a–e).

Differentiated endodermal cells have a distinct transcriptional auxin response. We interrogated the genome-wide transcriptional responses in *slr-1* and *CASP1pro::shy2-2/slr-1* after NAA treatment at multiple time points. We established that around 800–900 genes are differentially expressed at 2, 4, 8 and 16 h after treatment and around 1,000 are significantly changed after 24 h treatment compared with the zero timepoint (Supplementary Table 1). Using non-supervised methods and manual tests, we settled on seven clusters to describe the data (Fig. 1f,g). As expected, the dataset contained a large number of cell wall-related genes and hardly any cell cycle-related genes. Analysing the gene ontology (GO) annotations, we observed terms linked to auxin signalling and lateral root development (clusters 2 and 5), whereas terms related to lipid transport and fatty acid metabolism were enriched in clusters 3 and 5. The fact that we observed few GO terms related solely to auxin signalling and lateral root development is most probably a result of the experimental design, which provides an auxin-response profile focused on a specific, differentiated cell type. To substantiate this proposition, we compared the *slr-1* versus *CASP1pro::shy2-2/slr-1* data with the two previously published datasets from transcriptome analyses dealing either with roots treated with auxin or microdissected root sections after gravistimulation-mediated lateral root induction[14,15]. There appeared to be little correlation between the differentially expressed genes in our dataset and those in the datasets of Lewis et al.[14] or Voß et al.[15] (Extended Data Fig. 2b,c), confirming the distinct and specific nature of this transcriptional profile. To identify genes involved in cell wall modification, as well as to confirm the validity of our transcriptional profile, we selected a wide range of genes possibly related to the observed endodermal responses, including genes linked to lignification or lipid transport, as well as several unknown genes showing particularly strong and high-confidence differential responses. We generated promoter–reporter lines to characterize their expression pattern during root development and lateral root formation. In a strong validation of our approach, 24 out of 27 of the selected genes were found to display auxin-regulated expression in the endodermis (Extended Data Fig. 3 and Supplementary Table 2). A selection of these candidates (with constitutive or induced expression during lateral root formation) is shown in Extended Data Fig. 3c.

Many suberization-associated genes respond to auxin in the endodermis. Since we were interested in possible cell wall modifying enzymes, we searched the list of differentially expressed genes for cell wall-associated functions. We found that many genes with functions attributed to cutin or suberin homeostasis showed highly dynamic, differential expression in our dataset (Extended Data Fig. 3e). Suberin deposition has been shown to be highly plastic and might be continuously turned over, both for adaptation to the soil environment and during lateral root development[6–8]. Because we still lack an understanding of suberin deposition and turnover in the apoplast, we investigated whether some of the cell wall-related differentially expressed genes could be involved in this process. In particular, we were intrigued by the high number of differentially expressed GDSL-type esterase/lipase proteins (GELPs) in our dataset (Extended Data Fig. 3e), since members of this large family have been shown to be involved in cutin polymerization and to be able to degrade both cutin and suberin[16–20]. We therefore focused on the differentially regulated set of GELPs.

Concomitant suberin degradation and lateral root cap cuticle formation during lateral root formation. Fluorol yellow staining reveals dynamic changes during lateral root formation. However, fluorol yellow stains both suberin and cutin[21] (Extended Data Fig. 6a), and it remains unclear if, how and at which stage endodermal suberin is degraded and a cutin-like structure is formed at the surface of the primordium. Therefore, we analysed the dynamics of suberin and cutin during lateral root formation using transmission electron microscopy (TEM) (Fig. 2). Analysing stage II lateral root primordia, which usually form in the unsuberized zone, we could detect suberin lamellae only in the endodermal cell walls facing the lateral root primordia, but not in the cell walls on the opposite side of the root (Fig. 2a). Stage III primordia are found in the patchy suberized zone of the root and, as expected, we detected both suberized and non-suberized endodermal cells. At this stage, we began to distinguish the onset of the lateral root cap cuticle formation, accompanied by the disappearance of suberin in the endodermal cell walls overlying the primordium (Fig. 2b). In stage IV primordia, which are usually found in the fully suberized zone, we detected suberin deposition in all endodermal cells in zones without a primordium. At the same time, it was difficult to observe any suberin in endodermal cells facing the primordia. Indeed, it appeared as if suberin was degraded in coordination with the formation of the root cap cuticle (Fig. 2c). In fully emerged lateral roots, we could

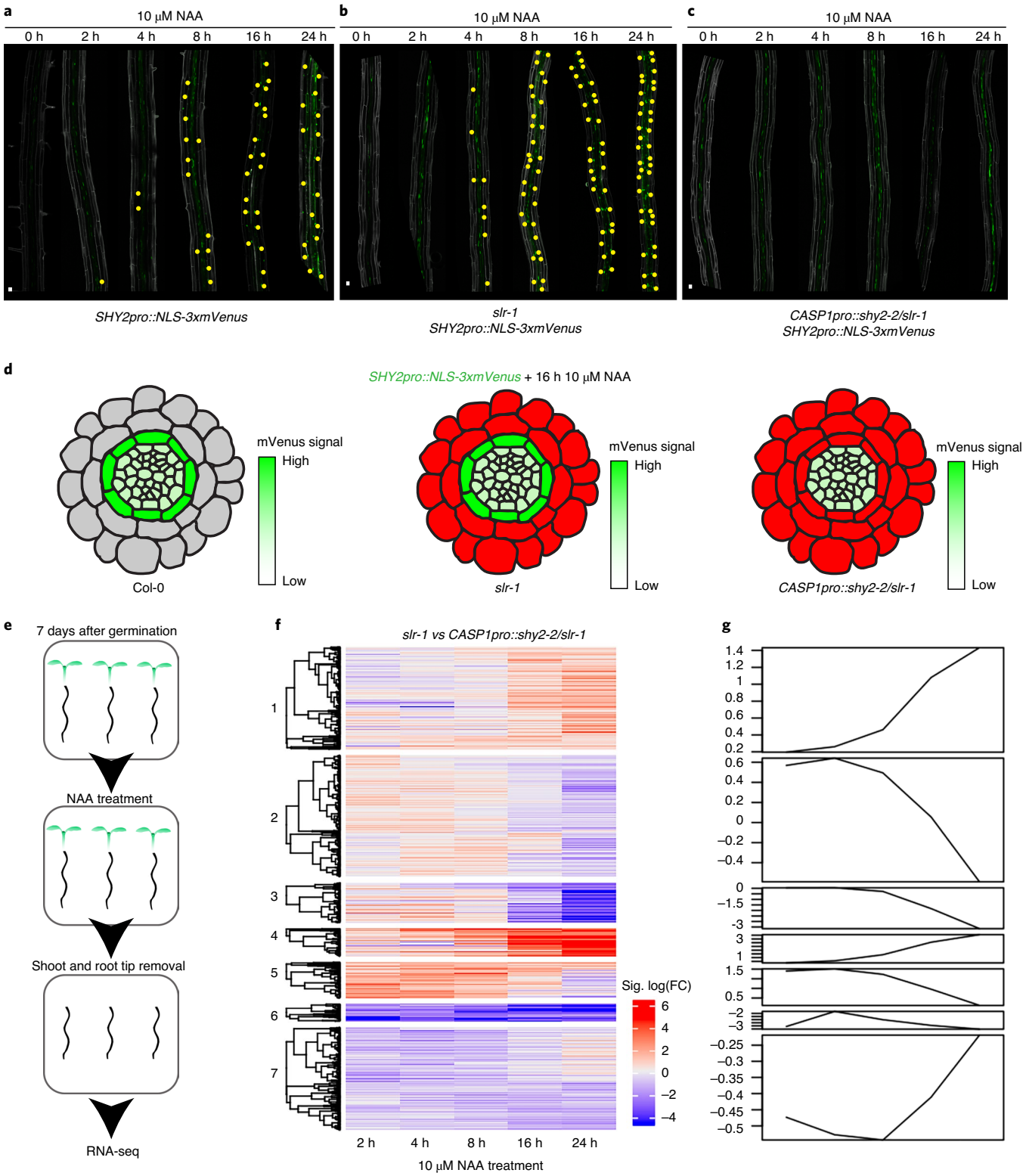

Fig. 1 | Using genetics to map auxin responses in the differentiated endodermis. a–c, Maximum intensity projections of roots expressing *SHY2pro::NLS-3xmVenus* treated with 10 μM NAA for 0, 2, 4, 8, 12 and 24 h. **a**, Col-0. **b**, *slr-1*. **c**, *CASP1pro::shy2-2/slr-1*. Yellow dots indicate *SHY2pro::NLS-3xmVenus* signal in the endodermis. Further details are provided in Extended Data Fig. 1. Images are representative of experiments repeated three times. **d**, Schematic representation of *SHY2pro::NLS-3xmVenus* responses in the different genetic backgrounds after treatment with 10 μM NAA for 16 h. *SHY2pro::NLS-3xmVenus* signal is indicated in green and inhibition of auxin signalling by *slr-1* or *CASP1pro::shy2-2* is indicated in red. **e**, Experimental setup of the RNA-seq experiment. **f**, Heat map showing the seven clusters containing the significant differentially expressed genes (cut-off fold change (FC) >2, false discovery rate <0.05) between roots of *slr-1* and *CASP1pro::shy2-2/slr-1* plants during the time course of NAA treatment. **g**, Graphical presentation of the behaviour of the seven clusters during the NAA time course depicted in **e**. Scale bars in **a–c,** 50 μm.

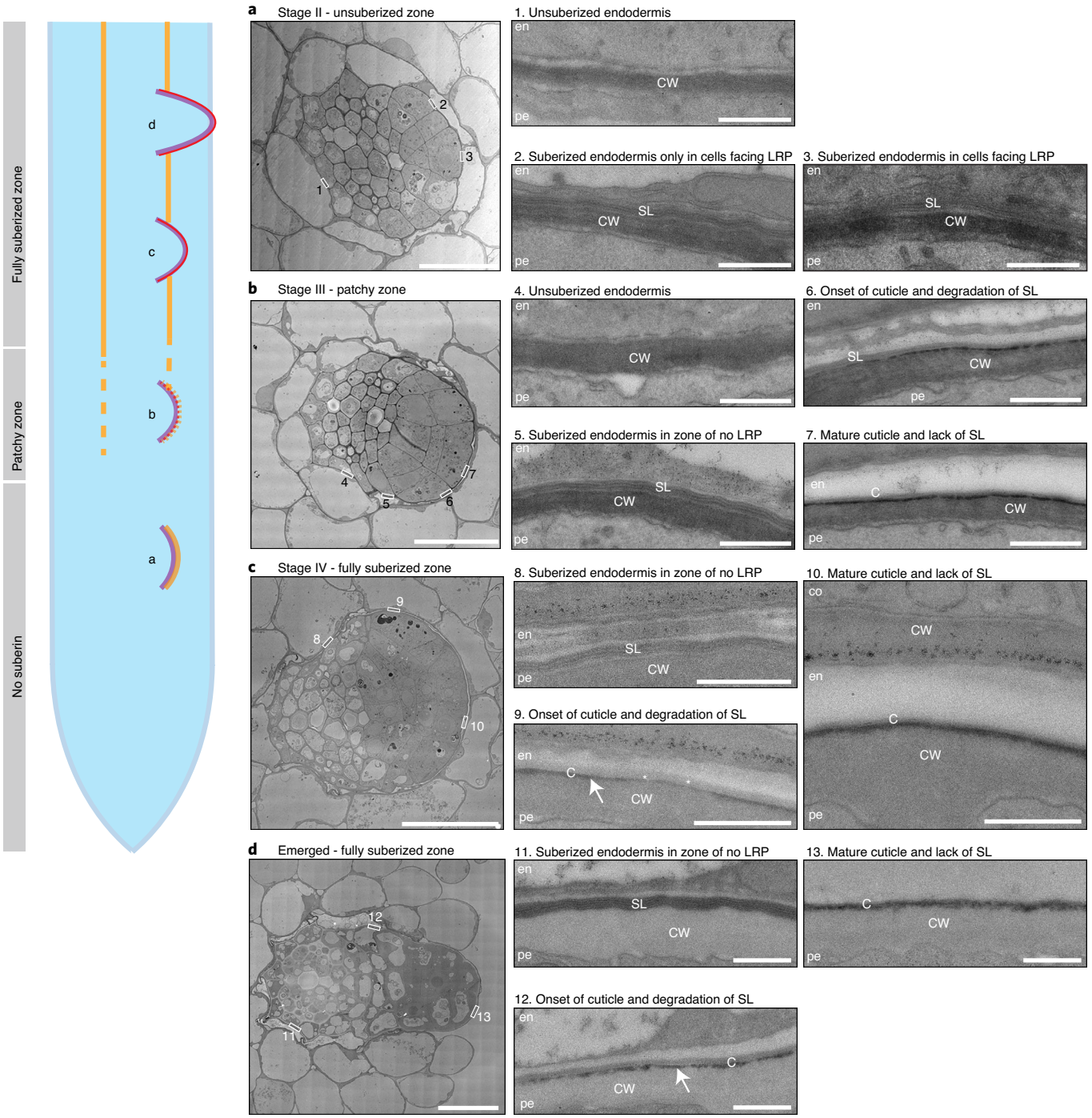

Fig. 2 | Suberin is degraded while the lateral root cap cuticle is established during lateral root formation. a–d, TEM micrographs of root sections containing stage II (**a**), stage III (**b**) and stage IV (**c**) lateral root primordia (LRP) and emerged lateral root (**d**). The numbered boxed regions are magnified on the right. Each experiment was repeated three times. The root schematic indicates the different stages of lateral root development shown in **a–d**. Purple, outline of lateral root primordium; yellow, suberin; red, cutin; en, endodermis; pe, pericycle; co, cortex; SL, suberin lamellae; C, lateral root cap cuticle; CW, cell wall. Arrows in panel 9 and 12 indicate the forming lateral root cap cuticle. Scale bars: 10 µm (**a–d**, main image); 1 µm (**a–d**, magnified images 1–12).

detect only the lateral root cap cuticle, whereas endodermal cells not in contact with the primordium still maintained their suberin lamellae (Fig. 2d). Thus, our analysis reveals that suberin is gradually degraded in cell walls of endodermal cells overlying the lateral root primordium, concomitant with the synthesis of a lateral root cap cuticle in the primordium as a protective coating[21].

Expression of auxin-repressed GELPs strongly correlates with endodermal suberization. To our knowledge, no factors mediating suberin polymerization[22] have been identified. Currently, the strongest available interference with suberin biosynthesis in roots relies on either endodermis-specific interference with abscisic acid (ABA) or cytokinin signalling, artificial overexpression of a cutin-degrading

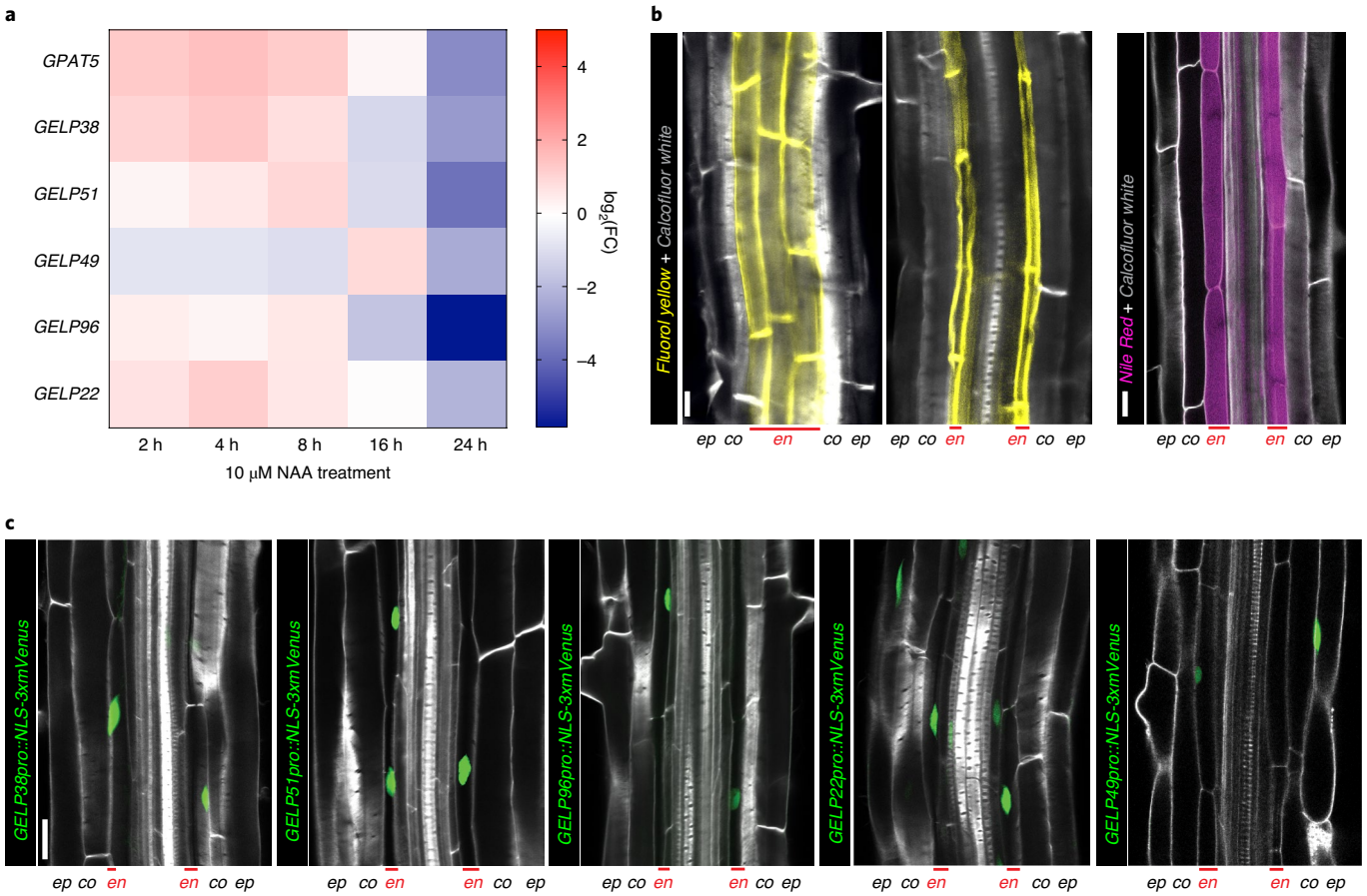

Fig. 3 | A cluster of five auxin-repressed GELPs is expressed in the differentiated endodermis. a, Heat map showing the differential expression of *GPAT5*, *GELP38*, *GELP51*, *GELP49*, *GELP96* and *GELP22* during the time course of NAA treatment (10 µM). **b**, Representative image of staining of suberin lamellae in the endodermis using fluorol yellow (yellow) or Nile red (magenta). ep, epidermis; co, cortex; en, endodermis. **c**, Confocal images of root sections expressing transcriptional reporters for each of the GELPs mentioned in **a**. NLS–3xmVenus is shown in green, calcofluor white staining of cell walls in grey. Each experiment was repeated three times. Scale bars in **b**,**c**, 25 µm.

enzyme or tissue-specific manipulation of phenylpropanoid production[6,7,18,23]. *CUTIN DEFICIENT 1* (*CD1*), a member of the large family of GELP proteins[20], has been shown to have in vitro cutin synthase activity, and CD1 loss-of-function mutants in tomato show partial defects in cuticle formation, but no equivalent evidence exists for suberin synthases. We observed a group of five GELP genes (*GELP22*, *GELP38*, *GELP49*, *GELP51 and GELP96*) to be downregulated after prolonged auxin treatment (Fig. 3a). Since auxin treatment should downregulate suberin-biosynthetic enzymes during lateral root formation[8], we speculated that the five downregulated GELPs might have a role in suberin biosynthesis. This idea was corroborated by the expression of transcriptional reporters for *GELP22*, *GELP38*, *GELP49*, *GELP51* and *GELP96*. *GELPXpro::NLS-3xmVenus* reporter lines revealed endodermis-specific expression for *GELP38*, *GELP51* and *GELP96*, and expression in endodermis and epidermis for *GELP22* and *GELP49* (Fig. 3c). Since treatment of *Arabidopsis* seedlings with ABA and CASPARIAN STRIP INTEGRITY FACTOR 2 (CIF2) peptide results in increased suberin deposition and *GPAT5* marker expression[7,24,25], we further checked whether *GELP22*, *GELP38*, *GELP49*, *GELP51* and *GELP96* would be induced by treatment with ABA and CIF2. All *GELP* reporter lines were induced in response to these treatments and also expanded their expression domain into the cortex, similar to what has been reported for *GPAT5*[7] and (Extended Data Fig. 4a,b). Together, our data establishes a strong correlation between suberin biosynthesis and the expression pattern of these five GELPs.

Suberin deposition requires auxin-repressed GELPs. To establish a function for these GELPs in suberin biosynthesis, we collected available transfer DNA (T-DNA) insertion mutants and characterized them for differences in suberin deposition using fluorol yellow or Nile red, two fluorescent dyes that stain suberin (Fig. 3b). In the absence of T-DNA insertion lines for *GELP38*, we generated two loss-of-function mutants using clustered regularly interspaced short palindromic repeats (CRISPR)–CRISPR-associated protein-9 nuclease (Cas9) (CRISPR–Cas9). None of the single mutants showed any significant difference in suberin occupancy in *Arabidopsis* roots compared to wild-type (Extended Data Fig. 4c–e). Using CRISPR–Cas9, we then generated two different allelic combinations of the five putative suberin biosynthesis-related GELPs: *gelp22-c1/gelp38-c3/gelp49-c1/gelp51-c1/gelp96-c1* and *gelp22-c2/gelp38-c4/gelp49-c2/gelp51-c2/gelp96-c2* (hereafter called $gelp^{quint\text{-}1}$ and $gelp^{quint\text{-}2}$, respectively) (Extended Data Fig. 4f). To test whether suberin levels in roots of the $gelp^{quint\text{-}1}$ and $gelp^{quint\text{-}2}$ mutants were affected, we stained roots of five-day-old plants with fluorol yellow and Nile red. Whereas suberin staining in wild-type plants resulted in the described patterns[18], both quintuple mutants showed a complete absence of suberin staining (Fig. 4a–d and Extended Data Fig. 5a). ABA treatment is known to strongly enhance suberization both in endodermis and cortex[7]. Yet, even after ABA induction, no suberin deposition could be detected using fluorol yellow staining in the roots of $gelp^{quint\text{-}1}$ and $gelp^{quint\text{-}2}$ plants (Fig. 4e,f). CIF2 peptide

did also not enhance suberization in *gelp*$^{quint-1}$ plants (Extended Data Fig. 5c). Since cutin and suberin can both be stained by fluorol yellow, we investigated whether the lateral root cap cuticle was affected in roots of the *gelp*$^{quint-1}$ mutant. We found that fluorol yellow still stained the dome of the emerging lateral root, suggesting that the *gelp*^{quint} mutants are specifically affected in suberization, leaving the lateral root cap cuticle intact (Fig. 4g,h). This was confirmed by TEM analysis (Extended Data Fig. 5d). Since endodermal suberin was shown to interfere with uptake from the apoplast, we used the fluorescein diacetate (FDA) penetration assay[7] to test for the presence of functional suberin lamellae in the endodermis of *gelp*^{quint} roots. Whereas FDA could enter only the epidermis and cortex in the suberized zone of wild-type roots, it entered the endodermis of *gelp*^{quint} roots, demonstrating absence or a strong deficiency of the endodermal suberin barrier (Extended Data Fig. 5e). To directly measure suberin levels, we performed a chemical analysis of the suberin content in roots of wild-type and *gelp*^{quint} mutants. This revealed substantial reductions in the amount of aliphatic suberin monomers in both *gelp*$^{quint-1}$ and *gelp*$^{quint-2}$ mutants, with nearly identical patterns in both allelic combinations. Dicarboxylic acids were nearly absent (98% reduction), whereas ω-hydroxy acids and fatty alcohols were reduced by about 90% and 50%, respectively (Fig. 4i). Ferulates were reduced by 70%, whereas coumarates showed only minor reductions. This resulted in an overall reductions of about 85% in the amount of suberin monomers compared with wild-type roots (Fig. 4i), correlating well with the fluorol yellow staining. Next, we complemented the suberin phenotype of the *gelp*$^{quint-1}$ mutant by introducing an inducible *GELP38proXVE>>GELP38-mCITRINE* fusion into the *gelp*$^{quint-1}$ mutant. This restored the stereotypical fluorol yellow staining in roots, demonstrating functionality of the GELP38–mCITRINE protein (Fig. 4j,k). The complementation was further confirmed using TEM analysis (Extended Data Fig. 5g). Moreover, GELP38–mCITRINE was localized in the apoplast of the endodermis where suberin polymerization takes place (Fig. 4l and Extended Data Fig. 5f). We also tested whether the Casparian strip was unaffected in the *gelp*^{quint} mutants and found both lignin staining with basic fuchsin and uptake of propidium iodide to be unaffected (Extended Data Fig. 5h–j). Thus, a cluster of five auxin-repressed GELPs is essential for normal suberin deposition in the endodermis, but does not affect lateral root cap cuticle formation.

Finally, using TEM, we could readily detect suberin lamellae in endodermal cell walls of wild-type, but did not see any indication of lamellae formation in roots of *gelp*$^{quint-1}$ (Fig. 4m,n and Extended Data Fig. 5b). Instead, we observed a layer of low electron density in the cell wall of the *gelp*$^{quint-1}$ mutant (Fig. 4m,n and Extended Data Fig. 5b). This layer appears amorphous with no resemblance to the lamellar structures in the wild-type. We speculate that this layer might be formed due to the accumulation of unpolymerized suberin monomers in the mutant cell wall. Together, our results strongly support an absence of suberin in the endodermis of the *gelp*^{quin1} mutant.

The *gelp*^{quint} mutants show expected defects of a suberin-deficient mutant. Since it has been repeatedly demonstrated that roots with non-functional suberin barriers are more susceptible to elevated salt concentrations, we also subjected 4-day-old seedlings to a mild salt stress (85 mM NaCl) for 8 days. Both *gelp*^{quint} mutants were more affected by the salt stress compared with the wild type (Extended Data Fig. 5k–m). We observed fewer emerged lateral roots and the fresh weight of the shoot was also significantly reduced (Extended Data Fig. 5k–m). These observations again strongly support the absence of a functional suberin barrier in the *gelp*^{quint} mutants. We finally checked whether the expression of known suberin biosynthesis-related genes was altered in the *gelp*^{quint} mutants. None of these genes were differentially expressed in the *gelp*^{quint} mutants (Extended Data Fig. 5n). This excludes the possibility that the observed absence of suberin would be due to an indirect feedback regulation of suberin biosynthesis and supports a direct role for the five GELPs in suberin polymerization in the apoplast.

Some auxin-induced GELPs have the capacity to degrade suberin. We also identified a group of five GELPs (*GELP12*, *GELP55*, *GELP72*, *GELP73* and *GELP81*) that were induced by auxin (Fig. 5a). Our RNA-sequencing (RNA-seq) data revealed that expression of *GELP12*, *GELP55* and *GELP72* peaks after 24 h of NAA treatment, whereas expression of *GELP73* and *GELP81* peaks after about 4 h (Fig. 5a). Expression of GELP12, GELP55 and GELP72 reporters show specific induction in endodermis during lateral root formation, whereas *GELP73* and *GELP81* reporters display endodermal expression already before lateral root formation (Fig. 5e and Extended Data Fig. 6f,g). Since we and others have demonstrated that the endodermal suberin gradually disappears, while a layer of cutin is formed at the primordium[16,21] (Fig. 2 and Extended Data Fig. 6a), we hypothesized that in contrast to the auxin-repressed suberin-biosynthetic GELPs, the five auxin-induced GELPs could regulate removal of suberin. First, we confirmed removal of suberin by other fluorescent staining methods besides fluorol yellow and found that both auramine O and Nile red can be used to visualize suberin in differentiated roots and both confirmed local degradation of suberin in cells overlying the lateral root (Fig. 5b,c). We also assessed suberin staining in the *bodyguard* mutant. BODYGUARD is an α/β-hydrolase that has been implicated in the establishment of the root cap cuticle[21], but it is not clear whether it affects endodermal suberin accumulation. Fluorol yellow staining in *bodyguard* roots confirmed the effect on lateral root cap cuticle, but suberin degradation appears to be normal and even more easily observable in this mutant, due to the lack of cuticle staining (Fig. 5d and Extended Data Fig. 6b,c). When characterizing the expression patterns of the five putatively suberin-degrading

Fig. 4 | Suberin deposition requires a cluster of auxin-repressed GELPs. a, Confocal images of Col-0 seedling roots stained with fluorol yellow. **b**, Confocal images of *gelp*$^{quint-1}$ and *gelp*$^{quint-2}$ seedling roots stained with fluorol yellow. Note absence of fluorol yellow staining. **c**,**d**, Close-up image of root sections of Col-0 (**c**) or *gelp*$^{quint-1}$ and *gelp*$^{quint-2}$ (**d**) stained with fluorol yellow for suberin and calcofluor white for cell walls. **e**,**f**, ABA-induced increased suberin deposition in Col-0 roots (**e**) but not in roots of *gelp*$^{quint-1}$ and *gelp*$^{quint-2}$ mutants (**f**). **g**,**h**, Fluorol yellow staining of Col-0 (**g**) and *gelp*$^{quint-1}$ (**h**) roots, showing that the cuticle layer protecting emerging lateral roots appears to be unaffected in the *gelp*$^{quint-1}$ mutant. Each experiment in **a**–**h** was repeated at least three times. **i**, Chemical analysis of the suberin content in roots of wild-type and *gelp*$^{quint-1}$ or *gelp*$^{quint-2}$ reveals a decrease of about 85% in total suberin monomers. Quantification of aliphatic and aromatic ester-bond suberin monomers isolated from six-day-old roots of wild-type (Col-0) and *gelp*$^{quint-1}$ and *gelp*$^{quint-2}$ mutants. The graph shows the analysis of the principal suberin monomers and the inset shows the total monomers per genotype. Data are mean ± s.e.m.; $n = 4$. Analysis of variance (ANOVA) and Tukey test: $^{***}P < 0.001$, $^{**}P < 0.01$, $^{*}P < 0.05$, NS, not significant. DCA, dicarboxylic acid; ω, ω-hydroxy acid; FA, fatty alcohol. **j**,**k**, Induction of *GELP38-XVEpro::GELP38-mCITRINE* restores suberin deposition in the roots of *gelp*$^{quint-1}$. **l**, Confocal image of a root expressing *GELP38-XVEpro::GELP38-mCITRINE* (green) after β-oestradiol treatment (5 μM) stained with Nile red (magenta) for suberin and calcofluor white (grey) for cell walls. **m**,**n**, TEM micrographs of root cross sections showing presence of suberin lamellae in wild-type roots (**m**) and absence of suberin lamellae in cross sections of *gelp*$^{quint-1}$ roots (**n**). Note that the structure of the endodermis of the *gelp*$^{quint-1}$ mutant is much better preserved compared to wild-type. Images in **j**–**n** are representatives of experiments that were repeated three times. Scale bars: 500 μm (**a**,**b**,**e**,**f**,**j**); 25 μm (**c**,**d**,**g**,**h**,**k**,**l**); 10 μm (**m**,**n**, whole root sections); 20 nm (**m**,**n**, magnified regions).

GELPs, we observed three different expression patterns. *GELP12* and *GELP55* marker lines showed expression in the cortex or no signal in absence of lateral root formation, but were induced in endodermal cells overlying the lateral root from stages I to IV (Fig. 5e and Extended Data Fig. 6d). *GELP72* was induced in endodermal cells overlying the lateral root primordium and from stage III onwards,

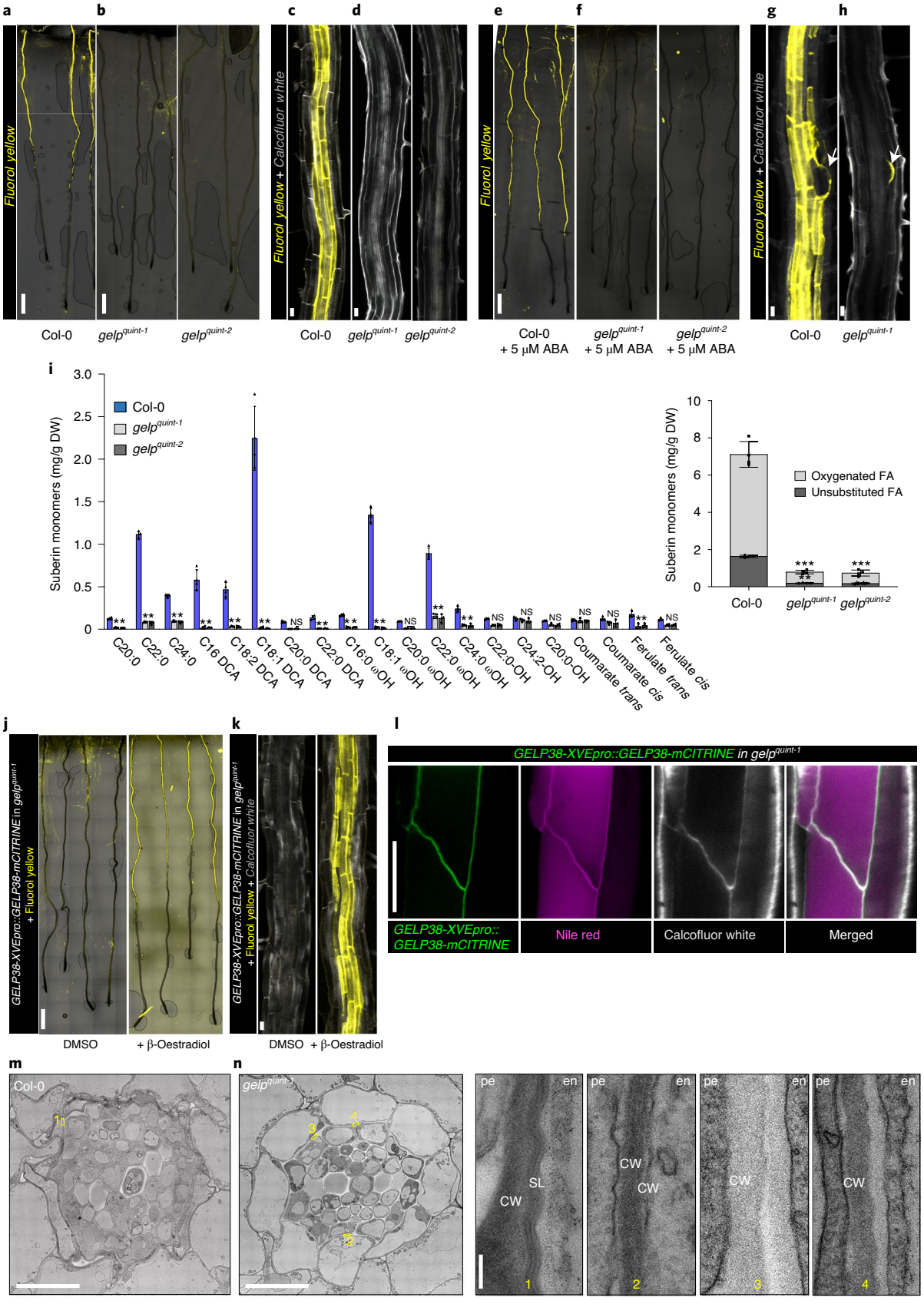

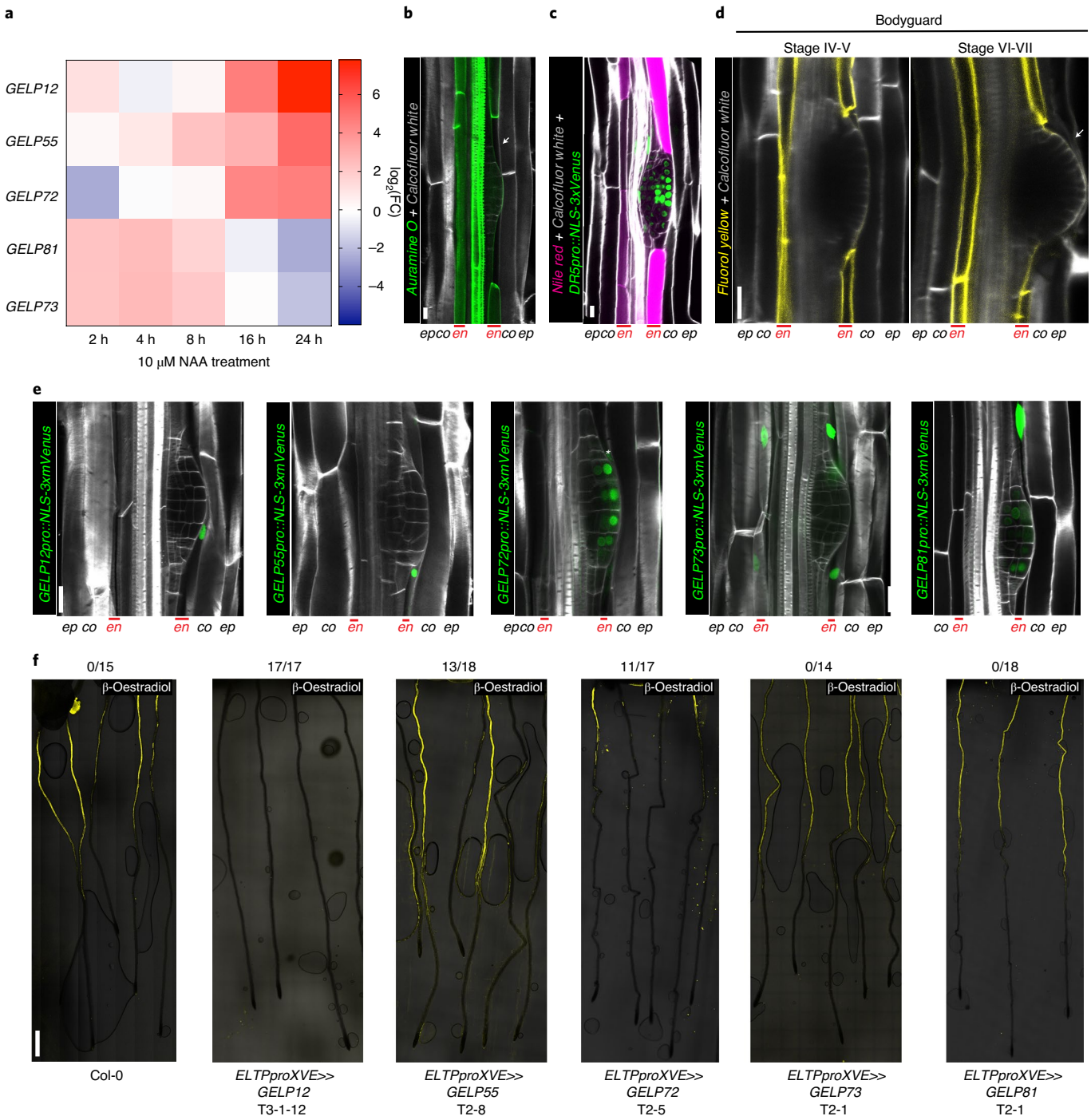

Fig. 5 | A cluster of auxin-induced GELPs is required for suberin degradation. a, Heat map showing the differential expression of *GELP12*, *GELP55*, *GELP72*, *GELP81* and *GELP73* during the 10 μM NAA time course. **b**, Use of auramine O (green) to visualize degradation of suberin in the cell wall of endodermal cells overlying a lateral root primordium. **c**, Use of Nile red staining (magenta) to visualize suberin degradation in the cell wall of endodermal cells overlying a lateral root primordium. Auxin signalling is visualized by *DR5pro::NLS-3xVenus* (green). **d**, Fluorol yellow staining in roots of *bodyguard* mutant, demonstrating normal presence of suberin lamellae, whereas the cuticle layer surrounding the lateral root primordium is discontinuous (arrow). **e**, Confocal images showing the expression patterns of the isolated auxin-upregulated GELPs during lateral root formation. NLS-3xmVenus signal in green and calcofluor white staining of cell walls is in grey. Asterisk indicates endodermal signal. **f**, Fluorol yellow staining on roots of Col-0 treated with oestradiol results in normal suberin pattern, whereas inducible endodermis-specific overexpression of *GELP12*, *GELP55* or *GELP72* results in degradation of suberin highlighted by absence of fluorol yellow signal. The overexpression of *GELP73* and *GELP81* results in a normal suberin pattern similar to untreated wild-type roots. The numbers above the images indicate the number of roots without fluorol yellow staining/total number of imaged roots. Images in **b**–**f** are representative of experiments repeated at least three times. Scale bars: 25 μm (**b**–**e**); 500 μm (**f**).

and was also expressed in the outer layer of the growing primordium (Fig. 5e and Extended Data Fig. 6e). Finally, *GELP73* and *GELP81* were already expressed in the endodermis before lateral root initiation and were induced in the overlying endodermal cells from stages I to IV (Fig. 5e and Extended Data Fig. 6f,g). In addition, from stage IV onwards, *GELP81* was induced in the outer layer of the primordium, similarly to *GELP72* (Extended Data Fig. 6g). Confirming the RNA-seq data, GELP12, GELP55 and GELP72 marker lines were induced by auxin in an endodermis-specific fashion (Extended Data Fig. 6h–j). To characterize a possible role in suberin degradation, we first undertook a gain-of-function approach by inducibly overexpressing each GELP in the endodermis and assessing whether this causes suberin removal using fluorol yellow staining. Indeed, inducible expression of *GELP12*, *GELP55* and *GELP72* in the endodermis caused a disappearance of fluorol yellow staining, whereas no clear effect on fluorol yellow staining was observed when inducing *GELP81* and *GELP73* (Fig. 5f and Extended Data Fig. 7a,c). We also performed a transfer experiment in which we germinated the inducible lines with endodermis-specific expression of GELP12 on normal β-oestradiol-free medium for 4 d to allow suberin formation and then transferred the seedlings to the plates containing oestradiol for 36 h. We observed a clear reduction in root suberin (Extended Data Fig. 7b). We then tested whether single loss-of-function mutants of each individual GELP affects lateral root formation (Extended Data Figs. 7d and 8a–g). We performed root bending assays to synchronously induce lateral roots and to quantify the progression of lateral root development at 18 h and 42 h after gravistimulation[26,27]. Among the three GELPs that can degrade suberin, only one (GELP72) showed a delayed lateral root development in both alleles and time points (Extended Data Fig. 8d–g). However, the single mutants of the *GELP73* and *GELP81* genes—which did not affect fluorol yellow staining when overexpressed in the endodermis—also displayed a delayed lateral root emergence (Extended Data Fig. 8h–k). Thus, some auxin-inducible GELPs are able to degrade suberin when overexpressed and some also display single mutant phenotypes during lateral root emergence. Thus, while our data makes auxin-induced GELPs strong candidates for suberin degradases during lateral root emergence and suggests a need for suberin degradation for proper lateral root emergence, further efforts in generating and analysing multiple mutant combinations of these GELPs will be needed to clearly establish their role and the requirement for suberin degradation during this process.

Discussion

Our data reveal that differentiated endodermal cells have a distinct auxin-mediated transcriptome. Mining this unique auxin-response dataset enabled us to identify the first suberin synthase candidates (Figs. 1 and 3) and a set of candidate suberin degradases (Fig. 5). Together these enzymes appear to form a module for regulating suberin plasticity in roots. Knocking out all five suberin synthases resulted in roots without detectable suberin that are hypersensitive to mild stress conditions. These *gelp*^{quint} mutants provide the plant community with a powerful tool to test the role of suberin and its plasticity during diverse environmental conditions. It will be interesting to test how the loss of suberin affects interactions with microbiome and susceptibility to pathogen attack[1]. The strong quintuple mutant and the identification of suberin degradase candidates will also aid further understanding of the mechanisms and role of suberin plasticity in plant elemental homeostasis[7]. The large GELP family in *Arabidopsis* and other plants provides a rich, but as-yet untapped genetic resource, to better understand how different cell wall modifications affect biological processes and interactions.

Methods

Plant material and construction. For all experiments, *A. thaliana* ecotype Columbia (Col-0; wild-type) was used. Gene numbers, mutants and transgenic lines used and generated in this study are described in the Supplementary Information. The primers used for genotyping and quantitative PRC (qPCR)-based verification of T-DNA lines are indicated in Supplementary Table 5.

The following T-DNA tagged and transgenic lines were used in this study: *gelp49* (SALK_015138C), *gelp51* (SALK_033359C), *gelp96* (SALK056924C) and *gelp96* (SALK056924C) (NASC centre); *SHY2pro::NLS-3xmVenus*, *CASP1pro::shy2-2, DR5::NLS-3xVenus*[10]; *GPAT5pro::NLS-3xmVenus*[28] and *slr-1*[12] were described previously. The corresponding gene numbers are as follows: *SLR*, AT4G14550; *SHY2*, AT1G04240; *ELTP*, At2g48140; *GPAT5*, At3g11430; *SYP122*, At3g52400; BDG, AT1G64670; HORST, At5g58860; *ASFT*, At5g41040; *FAR1,* At5g22500; FAR4, At3g44540; *KCS2,* At1g04220; *GELP12*, AT1G28650; *GELP55*, AT2G30310; *GELP72*, AT3G48460; *GELP81*, AT4G26790; *GELP73*, AT3G50400; *GELP49*, AT2G19050; *GELP51*, AT2G23540; *GELP96*, AT5G37690; *GELP38*, At1G74460; *GELP22*, AT1G54000; *GELP103*, At5g45960; *PER10,* At1g49570; *PER11*, AT1G68850; *PER23*, AT2G38390; *PER28*, At3g03670; *PER55*, AT5G14130, *PER59*, At5g19890; *LAC2*, AT2G29130; *LAC12*, AT5G05390; *LAC13*, AT5G07130; LAC16, AT5G58910; *UCC1*, AT2G32300; *PLIP3,* AT3G62590; *CASPL4B1*, AT2G38480; *CASPL1A1*, AT1G14160; cytochrome b561 and DOMON domain-containing protein At4g17280; cytochrome b561 and DOMON domain-containing protein At5g47530.

Plant growth conditions. For all experiments, plants were germinated on solid half-strength Murashige and Skoog (MS) medium without addition of sucrose. Seeds were surface sterilized, sown on plates, incubated for 2 days at 4 °C for stratification, and grown vertically in growth chambers at 22 °C under continuous light (100 μE). The microscopic analyses (FDA uptake, fluorol yellow staining, propidium iodide uptake and confocal microscopy) were performed on 5- or 7-day-old seedlings.

Bending experiments. Seeds of wild-type Col-0 and *gelp* mutants were plated on half-strength MS containing 120 × 120 × 17 mm square Petri dishes, stratified in the dark at 4 °C for 2 days, and grown at 22 °C under constant light (100 μE). Lateral root stages were determined after plates with 4-day-old seedlings were rotated 90° and grown for 18 h and 42 h for synchronized lateral root induction. After bending for 18 h and 42 h, the roots were cleared as described in ref. [15] and mounted in 50% glycerol. Determination of lateral root stage in the bent region was done using an upright microscope with differential interference contrast optics. Experiments were repeated 3 times and each replicate had at least 15 seedlings.

Generation of transgenic lines. *CASP1pro::shy2-2* was crossed into the *slr-1* mutant to produce the *CASP1pro::shy2-2/slr-1* line. The In-Fusion Advantage PCR Cloning Kit (Clontech) and Gateway Cloning Technology (Invitrogen) were used for generating marker lines and overexpression constructs. All constructs were transformed by heat shock into *Agrobacterium tumefaciens* GV3101 strain and then transformed into plants by floral dipping[28]. At least ten independent transgenic lines were analysed for expression patterns, and one line showing a representative signal and normal segregation was selected for further studies. For transcriptional reporters, the promoter regions were PCR-amplified from Col-0 genomic DNA and cloned into pDONRP4-P1R (Thermo Fisher). The resulting plasmids were recombined together with pDONRL1-NLS-3xmVenus-L2 (ref. [29]) and the destination vector pFR7m24GW or pFG7m24GW, containing the FastRed or FastGreen cassettes for transgenic seed selection respectively, to create the final *PROMOTER::NLS-3xmVenus* expression clones. To be able to induce expression of individual GELPs in the endodermis, the corresponding pDONR221_ L1-GELP-L2 clones were created. The resulting clones were recombined with the oestradiol-inducible pDONR_P4-ELTPproXVE-P1R[23] and destination vector pB7m24GW, to produce *ELTPproXVE::GELP* overexpression lines. To generate *GELP38proXVE»GELP38:mCitrine*, the promoter region of GELP38pro was PCR-amplified from Col-0 genomic DNA and cloned into linearized p1R4-ML:XVE[30] with KpnI by Infusion cloning (Takara) to produce the inducible *GELP38proXVE* promoter clone. The resulting clone was recombined together with *pDONR221_L1-GELP38-L2*, *pDONR_R2-mCitrine-L3* and *pFG7m34GW* to produce the *GELP38proXVE»GELP38:mCitrine* construct. Supplementary Tables 3 and 4 shows details about the primers used for cloning. The spacers to customize sgRNA for SpCas9 were cloned using the oligo annealing technique, then ligated into BbsI linearized, Gateway-entry plasmids[31]. For multiplex targeting of GELP genes, the six sgRNAs utilized were cloned into two vectors, each carrying three sgRNAs and co-transformed together into Col-0 ecotype. The primers used for generating single and multiple CRISPR–Cas9 mutants are indicated in the Supplementary Table 7.

Hormonal treatments. ABA was stored as a 50 mM stock solution in methanol. When seedlings were subjected to short-term 10 μM ABA treatment, the transfer was done when the seedlings were four days old. β-oestradiol was prepared as 100 mM stock in DMSO. In the case of β-oestradiol treatment, seedlings were directly germinated on the medium containing 5 μM oestradiol. For salt experiments, the seedlings were grown on half-strength MS medium and transferred to 85 mM NaCl for 10 d. In the case of auxin (NAA) treatment for RNA-seq experiments, the seedlings were first grown on half-strength MS medium

and then transferred to 10 µM NAA for 4, 8, 16 or 24 h. At each time point, the shoots and the root tips were removed.

Chemical analysis of suberin. Chemical analysis of suberin was performed on six-day-old seedlings. Before analysis, we confirmed that the growth conditions did not affect the phenotype of *gelp*$^{quint\text{-}1}$ and *gelp*$^{quint\text{-}2}$ by fluorol yellow staining. We used the protocol for the determination of ester-bond lipids as described by Berhin et al.[21]. In brief, 200 mg of seeds were grown on nylon mesh (200 mm pore size). After 6 d, the roots were shaved off after flash freezing and extracted in isopropanol/0.01% butylated hydroxytoluene. They were then delipidized three times (at 1 h, 16 h and 8 h) in each of the following solvents: chloroform:methanol (2:1), chloroform:methanol (1:1) and methanol with 0.01% butylated hydroxytoluene, under agitation, before being dried for 3 d under vacuum. Depolymerization was performed by base catalysis[32]. In brief, dried plant samples were transesterified in 2 ml of reaction medium. Twenty millilitres of reaction medium was composed of 3 ml methyl acetate, 5 ml of 25% sodium methoxide in dry methanol and 12 ml dry methanol. The equivalents of 5 mg of methyl heptadecanoate and 10 mg of ω-pentadeca-lactone per sample were added as internal standards. After incubation of the samples at 60 °C for 2 h 3.5 ml dichloromethane, 0.7 ml glacial acetic acid and 1 ml 0.9% NaCl (w/v) Tris 100 mM pH 8.0 were added to each sample and subsequently vortexed for 20 s. After centrifugation (1,500*g* for 2 min), the organic phase was collected, washed with 2 ml of 0.9% NaCl, and dried over sodium sulfate. The organic phase was then recovered and concentrated under a stream of nitrogen. The resulting cutin monomer fraction was derivatized with N,O-Bis(trimethylsilyl) trifluoroacetamide:pyridine (1:1) at 70 °C for 1 h and injected out of hexane on a HP-5MS column (J&W Scientific) in a gas chromatograph coupled to a mass spectrometer and a flame ionization detector (Agilent 6890N GC Network systems). The temperature cycle of the oven was the following: 2 min at 50 °C, increment of 20 °C min^{-1} to 160 °C, of 2 °C min^{-1} to 250 °C and 10 °C min^{-1} to 310 °C, and held for 15 min. Three independent experiments were performed with four replicates for each genotype, respectively, and a representative dataset is presented. The amounts of unsubstituted C16 and C18 fatty acids were not evaluated because of their omnipresence in the plant and in the environment.

Fluorescence microscopy. Confocal laser-scanning microscopy images were obtained using either a Zeiss LSM 880 (with Zen 2.1 SP3 Black edition), Leica SP8 (with LasX 3.1.5.16308) or Leica SP8-MP (with LasX 3.5.6.21594) microscopes. For green and red fluorophores, the following excitation and detection windows were used. mVenus, GFP, fluorol yellow and FDA: 488 nm, 500–530 nm; mCITRINE: 496 nm, 505–530 nm; propidium iodide: 520 nm, 590–650 nm; calcofluor white: 405 nm, 430–485 nm; basic fuchsin/Nile red 561 nm, 600–630 nm. For multiphoton microscopy the following excitation and detection settings were used. mVenus, GFP, fluorol yellow and calcofluor white 960 nm, 435–485 nm (calcofluor white) and 500–550 nm (mVenus, GFP and fluorol yellow). Methods for imaging the Casparian strip lignin and propidium iodide penetration were previously described[25,33]. For visualization of FDA transport, chambered cover glasses (Thermo Scientific), were used where the roots were covered with a slice of agar and time-lapse imaging was performed immediately after the application of FDA.

Methanol-based fluorol yellow staining of suberin in combination with calcofluor white. For most experiments suberin lamellae were observed in five- or seven-day-old roots using fluorol yellow (FY 088, Santa Cruz Biotechnology) staining. Seedlings were incubated in methanol at room temperature for at least 3 d, stained with FY 088 (0.01%, methanol) for 1 h at room temperature, rinsed in methanol and counterstained with aniline blue (0.5%, methanol) at room temperature for 1 h in darkness, washed, and visualized using 1-well chambered cover glass (ThermoFisher Scientific, catalogue no. 155361). To combine with calcofluor white for cell wall staining, the seedlings were first incubated in calcofluor white solution (0.1%, in methanol) for 3 d and then stained with fluorol yellow as described above.

Electron microscopy. For chemical fixation, plants were fixed in 2.5% glutaraldehyde solution (Electron Microscopy Services) in 0.1 M phosphate buffer pH 7.4 for 1 h at room temperature and post-fixed in a fresh mixture of osmium tetroxide 1% (Electron Microscopy Services) with 1.5% potassium ferrocyanide (Sigma) in phosphate buffer for 1 h at room temperature. The samples were then washed twice in distilled water and dehydrated in ethanol solution (Sigma) at graded concentrations (30%, 40 min; 50%, 40 min; 70%, 40 min; and 100%, 2 × 1 h). This was followed by infiltration in Spurr resin (Electron Microscopy Services) at graded concentrations (Spurr 33% in ethanol, 4 h; Spurr 66% in ethanol, 4 h; Spurr 100%, 2 × 8 h) and finally polymerized for 48 h at 60 °C in an oven. For the multiple mutant, 50-nm-thick sections were cut transversally 2 mm below the hypocotyl–root junction, using a Leica Ultracut (Leica Mikrosysteme), picked up on a copper slot grid 2 × 1 mm (Electron Microscopy Services) coated with a polystyrene film (Sigma). For lateral roots, 50-nm-thick sections were cut longitudinally (transversally from main root). For high-pressure freezing, plants were fixed in 2.5% glutaraldehyde solution (Electron Microscopy Services) in 0.1 M phosphate buffer pH 7.4 for 1 h at room temperature and post-fixed in a fresh mixture of osmium tetroxide 1% (Electron Microscopy Services) with 1.5% potassium ferrocyanide (Sigma) in phosphate buffer for 1 h at room temperature. The samples were then washed twice in distilled water before a high-pressure freezing step. For the high-pressure freezing, 2-mm-long root pieces were cut below the hypocotyl junction region, and then placed in an aluminium planchet 3 mm in diameter with a 0.2 mm cavity (article 241, Wohlwend) filled with hexadecene (Merck) covered with a tap planchet (article 353, Wohlwend) and directly frozen under high pressure using a HPF Compact 02 (Wohlwend). The samples were then dehydrated and infiltrated with resin at low temperature using the Leica AFS2 freeze-substitution machine (Leica Mikrosysteme) with the following protocol: dehydration in 100% acetone (Sigma) at graded temperature (−90 °C, 10 h; −90 °C to −60 °C, 2 h; −60 °C, 8 h; −60 °C to −30 °C, 2 h; −30 °C, −3 h.) This was followed by infiltration in spurr resin (Electron Microscopy Services) at graded concentration and temperature (30%, −30 °C to 0 °C, 10 h; 66%, 0 °C to 20 °C, 10 h; 100%, 20 °C, 2 × 10 h) and finally polymerized for 48 h at 60 °C in an oven. Fifty-nanometre sections were cut transversally to the root, using a Leica Ultracut (Leica Mikrosysteme), picked up on a copper slot grid of 2 × 1 mm (Electron Microscopy Services) coated with a polystyrene film (Sigma). Micrographs and panoramic were taken with a transmission electron microscope FEI CM100 (FEI) at an acceleration voltage of 80 kV with a TVIPS TemCamF416 digital camera (TVIPS) using the software EM-MENU 4.0 (TVIPS). Panoramas were aligned with the software IMOD[34].

RNA-seq experiments. Seeds were surface-sterilized, sown on plates, incubated for 2 d at 4 °C for stratification, and grown vertically in growth chambers at 22 °C under continuous light (100 µE) for 6 d. For each biological replicate (3 in total) 60 seedlings from each genotype were transferred to plates (20 seedlings per plate) containing 1/2 MS medium supplemented with 10 µM NAA and transferred back into the growth chamber. After the desired incubation period (2, 4, 8, 16 and 24 h) seedlings were harvested after removal of the root apical meristem (~3 mm) and the shoot including hypocotyl was snap-frozen in liquid nitrogen. RNA was extracted using a Trizol-based method. After RNase-free DNase (QIAGEN) treatment, RNA was cleaned-up using a RNeasy mini-elute kit (QIAGEN http://www.qiagen.com). RNA-seq libraries were prepared as described[35]. In brief, RNA quality was assessed on a Fragment Analyser (Advanced Analytical Technologies). RNA-seq libraries were prepared using 1,000 ng total RNA and the Illumina TruSeq Stranded mRNA reagents (Illumina) on a Sciclone liquid-handling robot (PerkinElmer) using a PerkinElmer-developed automated script. Cluster generation was performed with the resulting libraries using the Illumina TruSeq SR Cluster Kit v4 reagents and sequenced on the Illumina HiSeq 2500 using TruSeq SBS Kit v4 reagents. Sequencing data were processed using the Illumina Pipeline Software v.2.2.

RNA-seq data processing and analysis. Data processing was performed by the Lausanne Genomic Technologies Facility using their in-house RNA-seq pipeline. Data analysis was done using an in-house RNA-seq pipeline that performed the following steps. Quality controls were applied for cleaning data for adapters and trimming of low-quality sequence ends. Cleaned data was aligned and read counts computed using two methods: STAR[36] + HTSeq[37] and STAR + RSEM[38]. The first method generates gene counts and the second method generates isoform counts. TAIR10 genome and Ensembl 21 annotation were used. Additional quality controls were performed using R to inspect the sample counts summary, pairwise sample correlations, clustering and sample PCA. Statistical analysis was performed for genes and isoforms with the Bioconductor package EdgeR (R v.3.4.0) for normalization and limma (R v.3.18.2) for differential expression. Two types of statistical tests were applied depending on the contrast model tested. A moderated *t*-test was used for each pairwise comparison in group t0 and group *slr-1* vs *CASP1pro::shy2-2*/*slr-1*. A moderated *F*-test was used for each time-course model and their interaction. The result files contain one row per gene or transcript. Adjusted *P*-values were computed for each comparison by the Benjamini–Hochberg method, controlling for false discovery rate. Genes were considered significant in further analysis if the adjusted *P*-value was equal or below 0.05 and the $\log_2$-fold change was ≥ 1. Further analysis has been conducted using R (v.3.4.1). Heat maps were generated using ComplexHeatmap[39] (v.1.14.0) using Pearson distance, and 'average' for clustering. Non-supervised clustering of genes using kmeans (factoextra v.1.0.4; https://github.com/kassambara/factoextra)-suggested 3 clusters as optimal together. This represented a low resolution and we examined into clusters of size 4–8, which contained slightly lower silhouette values. After testing multiple cluster suggestions manually we settled on 7 inferred clusters based on the biologically most sensible separation. GO analysis was conducted using the package topGO v. 2.28.0 (weight01 algorithm[40]). GO annotations were obtained through org.At.tairGO (v.3.4.1). For the comparison with Lewis et al.[14], the published series matrix file was obtained from the Gene Expression Omnibus archive and the differential gene-expression analysis was repeated in order to obtain the expression of all genes. Results were compared with their published table of differentially expressed genes and found to be highly similar. A *z*-score based on the log (fold change) value was calculated for both our datasets and the reanalysed Lewis et al. data[14] to make the different datasets more comparable. For the comparison with Voß et al.[15], we used the published table directly; this table

included all expressed genes and calculated z-scores for the different time points. We kept time points T0, T6, T9, T15 and T24, which resulted in 7,145 differentially regulated genes with similar cut-off of $P < 0.05$ and a fold change of 2.

qPCR analysis. For qPCR quantifications, plants were grown on plates with half-strength MS medium covered with mesh. In the case of quintuple *gelp* mutants, only root parts (around 100 mg) were collected and total RNA was extracted using a Trizol-adapted ReliaPrep RNA Tissue Miniprep Kit (Promega). To verify the transcript level in single T-DNA lines, RNA extraction from whole seedlings was performed. Reverse transcription was carried out with PrimeScript RT Master Mix (Takara). All steps were done as indicated in manufacturer's manual. The qPCR reaction was performed on an Applied Biosystems QuantStudio3 thermocycler using a Mesa Blue SYBR Green kit (Eurogentech). All transcripts were normalized to ADAPTOR PROTEIN-4 MU-ADAPTIN (AP4M) (AT4G24550) expression. All primers used for qPCR are shown in Supplementary Table 6.

High-resolution melting analysis of CRISPR mutants. The high-resolution melting method was used to screen for the mutants generated using the CRISPR–Cas9-based method. Genomic DNA of selected Cas9-free, T2 generation plants, was extracted using the cetyl trimethylammonium bromide DNA extraction method. The qPCR reaction was performed on Applied Biosystems QuantStudio3 thermocycler using a MeltDoctor HRM Master Mix, according to the manufacturer's indications (Applied Biosystems). HPLC-purified primers were used to generate an amplicon of around 200 base pairs. The results were analysed using High Resolution Melt Software v.3.1 (Thermo Fisher Scientific). The selected candidates were verified by sequencing. Primers used for amplification and sequencing the potential mutation sites are indicated in Supplementary Tables 8 and 9.

Quantification and statistical analysis. For quantifying the fluorol yellow occupancy, confocal images were analysed with the Fiji package (v.2.0.0-rc-69/1.52p (build: 269a0ad53f); http://fiji.sc/Fiji)[41]. Contrast and brightness were adjusted in the same manner for all images. The suberized regions of the roots were measured together with total root lengths to determine the percentage of suberin occupancy. All statistical analyses were done with the GraphPad Prism software v.9.0.0 (86) (https://www.graphpad.com/) or using the R package (v.3.5.1) (http://www.r-project.org). One-way ANOVA was performed, and a two-sided t-test was subsequently used as a multiple-comparison procedure. For the analysis of lateral root development using the bending assay, we used a Pearson's χ^2 test. Details about the statistical approaches used can be found in the figure legends. The data are presented as mean ± s.d. or mean ± s.e.m. where indicated, and n represents the number of plant roots. Each experiment was repeated at least three times.

Reporting Summary. Further information on research design is available in the Nature Research Reporting Summary linked to this article.

Data availability

All data to support the conclusions of this manuscript are included in the main text and the supplementary materials. The full RNA-seq dataset was deposited in the NCBI Gene Expression Omnibus under accession GSE153478. Source data are provided with this paper.

Received: 17 July 2020; Accepted: 25 January 2021;
Published online: 08 March 2021

References

1. Castrillo, G. et al. Root microbiota drive direct integration of phosphate stress and immunity. *Nature* **543**, 513–518 (2017).
2. Duran, P. et al. Microbial interkingdom interactions in roots promote *Arabidopsis* survival. *Cell* **175**, 973–983 (2018).
3. Hassani, M. A., Duran, P. & Hacquard, S. Microbial interactions within the plant holobiont. *Microbiome* **6**, 58 (2018).
4. Banda, J. et al. Lateral root formation in *Arabidopsis*: a well-ordered LRexit. *Trends Plant Sci.* **24**, 826–839 (2019).
5. Stoeckle, D., Thellmann, M. & Vermeer, J. E. Breakout-lateral root emergence in *Arabidopsis thaliana*. *Curr. Opin. Plant Biol.* **41**, 67–72 (2018).
6. Andersen, T. G. et al. Tissue-autonomous phenylpropanoid production is essential for establishment of root barriers. *Curr. Biol.* (in the press).
7. Barberon, M. et al. Adaptation of root function by nutrient-induced plasticity of endodermal differentiation. *Cell* **164**, 447–459 (2016).
8. Li, B. et al. Role of LOTR1 in nutrient transport through organization of spatial distribution of root endodermal barriers. *Curr. Biol.* **27**, 758–765 (2017).
9. Yadav, V. et al. ABCG transporters are required for suberin and pollen wall extracellular barriers in *Arabidopsis*. *Plant Cell* **26**, 3569–3588 (2014).
10. Vermeer, J. E. et al. A spatial accommodation by neighboring cells is required for organ initiation in *Arabidopsis*. *Science* **343**, 178–183 (2014).
11. Tian, Q., Uhlir, N. J. & Reed, J. W. *Arabidopsis* SHY2/IAA3 inhibits auxin-regulated gene expression. *Plant Cell* **14**, 301–319 (2002).
12. Fukaki, H., Tameda, S., Masuda, H. & Tasaka, M. Lateral root formation is blocked by a gain-of-function mutation in the SOLITARY-ROOT/IAA14 gene of *Arabidopsis*. *Plant J.* **29**, 153–168 (2002).
13. Swarup, K. et al. The auxin influx carrier LAX3 promotes lateral root emergence. *Nat. Cell Biol.* **10**, 946–954 (2008).
14. Lewis, D. R. et al. A kinetic analysis of the auxin transcriptome reveals cell wall remodeling proteins that modulate lateral root development in *Arabidopsis*. *Plant Cell* **25**, 3329–3346 (2013).
15. Voß, U. et al. The circadian clock rephases during lateral root organ initiation in *Arabidopsis thaliana*. *Nat. Commun.* **6**, 7641 (2015).
16. Bakan, B. & Marion, D. Assembly of the cutin polyester: from cells to extracellular cell walls. *Plants* **6**, 57 (2017).
17. Girard, A. L. et al. Tomato GDSL1 is required for cutin deposition in the fruit cuticle. *Plant Cell* **24**, 3119–3134 (2012).
18. Naseer, S. et al. Casparian strip diffusion barrier in *Arabidopsis* is made of a lignin polymer without suberin. *Proc. Natl Acad. Sci. USA* **109**, 10101–10106 (2012).
19. Philippe, G. et al. Ester cross-link profiling of the cutin polymer of wild-type and cutin synthase tomato mutants highlights different mechanisms of polymerization. *Plant Physiol.* **170**, 807–820 (2016).
20. Yeats, T. H. et al. The identification of cutin synthase: formation of the plant polyester cutin. *Nat. Chem. Biol.* **8**, 609–611 (2012).
21. Berhin, A. et al. The root cap cuticle: a cell wall structure for seedling establishment and lateral root formation. *Cell* **176**, 1367–1378 (2019).
22. Philippe, G. et al. Cutin and suberin: assembly and origins of specialized lipidic cell wall scaffolds. *Curr. Opin. Plant Biol.* **55**, 11–20 (2020).
23. Andersen, T. G. et al. Diffusible repression of cytokinin signalling produces endodermal symmetry and passage cells. *Nature* **555**, 529–533 (2018).
24. Doblas, V. G. et al. Root diffusion barrier control by a vasculature-derived peptide binding to the SGN3 receptor. *Science* **355**, 280–284 (2017).
25. Fujita, S. et al. SCHENGEN receptor module drives localized ROS production and lignification in plant roots. *EMBO J.* **39**, e103894 (2020).
26. Lucas, M., Godin, C., Jay-Allemand, C. & Laplaze, L. Auxin fluxes in the root apex co-regulate gravitropism and lateral root initiation. *J. Exp. Bot.* **59**, 55–66 (2008).
27. Péret, B. et al. Auxin regulates aquaporin function to facilitate lateral root emergence. *Nat. Cell Biol.* **14**, 991–998 (2012).
28. Clough, S. J. & Bent, A. F. Floral dip: a simplified method for *Agrobacterium*-mediated transformation of *Arabidopsis thaliana*. *Plant J.* **16**, 735–743 (1998).
29. Gasperini, D. et al. Multilayered organization of jasmonate signalling in the regulation of root growth. *PLoS Genet.* **11**, e1005300 (2015).
30. Siligato, R. et al. MultiSite Gateway-compatible cell type-specific gene-inducible system for plants. *Plant Physiol.* **170**, 627–641 (2016).
31. Fauser, F., Schiml, S. & Puchta, H. Both CRISPR–Cas-based nucleases and nickases can be used efficiently for genome engineering in *Arabidopsis thaliana*. *Plant J.* **79**, 348–359 (2014).
32. Li-Beisson, Y. et al. Acyl-lipid metabolism. *Arabidopsis Book* **11**, e0161 (2013).
33. Ursache, R., Andersen, T. G., Marhavy, P. & Geldner, N. A protocol for combining fluorescent proteins with histological stains for diverse cell wall components. *Plant J.* **93**, 399–412 (2018).
34. Kremer, J. R., Mastronarde, D. N. & McIntosh, J. R. Computer visualization of three-dimensional image data using IMOD. *J. Struct. Biol.* **116**, 71–76 (1996).
35. Jan, M., Gobet, N., Diessler, S., Franken, P. & Xenarios, I. A multi-omics digital research object for the genetics of sleep regulation. *Sci. Data* **6**, 258 (2019).
36. Dobin, A. et al. STAR: ultrafast universal RNA-seq aligner. *Bioinformatics* **29**, 15–21 (2013).
37. Anders, S., Pyl, P. T. & Huber, W. HTSeq—a Python framework to work with high-throughput sequencing data. *Bioinformatics* **31**, 166–169 (2015).
38. Li, B. & Dewey, C. N. RSEM: accurate transcript quantification from RNA-seq data with or without a reference genome. *BMC Bioinformatics* **12**, 323 (2011).
39. Gu, Z., Eils, R. & Schlesner, M. Complex heatmaps reveal patterns and correlations in multidimensional genomic data. *Bioinformatics* **32**, 2847–2849 (2016).
40. Alexa, A. & Rahnenfuhrer, J. topGO: enrichment analysis for gene ontology. R package version 2.38.1 (2019).
41. Schindelin, J. et al. Fiji: an open-source platform for biological-image analysis. *Nat. Methods* **9**, 676–682 (2012).

Acknowledgements

We thank C. Grefen and M. Barberon for insightful discussions about GDSL-domain-containing proteins, experimental approaches and stimulating discussions; and the Electron Microscopy Facility and Imaging Facility of the University of Lausanne and the Center of Microcopy and Image Analysis of the University of

Zurich for excellent service and support. Work in the Geldner laboratory was supported by an ERC Consolidator Grant (GA-N: 616228-ENDOFUN) and two consecutive SNSF grants (CRSII3_136278 and 31003A-156261). R.U. was supported by an EMBO Long-Term Fellowship (EMBO ALTF 1046-2015). Work in the Nawrath laboratory was supported by a Swiss National Science Foundation grant (no. 310030_188672/1). Work in the Vermeer laboratory was supported by grants from the Swiss National Science Foundation (Schweizerischer Nationalfonds zur Förderung der Wissenschaftlichen Forschung; PP00P3_157524 and 316030_164086), the Netherlands Organization for Scientific Research (Nederlandse Organisatie voor Wetenschappelijk Onderzoek; NWO 864.13.008) and support from the University of Neuchâtel.

Author contributions

R.U., N.G. and J.E.M.V. conceived, designed and coordinated the project. R.U., C.D.J.V.T., V.D.T., D.D.B., K.G., V.S., T.G.A. and J.E.M.V. performed all experimental work. E.S.-S., S.C. and S.P. analysed RNA-seq data. J.E.M.V. wrote the first draft of the manuscript. R.U., T.G.A., C.N., N.G. and J.E.M.V. revised the manuscript and all authors were involved in the discussion of the work.

Competing interests

The authors declare no competing interests.

Additional information

Extended data is available for this paper at https://doi.org/10.1038/s41477-021-00862-9.

Supplementary information The online version contains supplementary material available at https://doi.org/10.1038/s41477-021-00862-9.

Correspondence and requests for materials should be addressed to R.U., N.G. or J.E.M.V.

Peer review information *Nature Plants* thanks Owen Rowland and the other, anonymous, reviewer(s) for their contribution to the peer review of this work.

Reprints and permissions information is available at www.nature.com/reprints.

Publisher's note Springer Nature remains neutral with regard to jurisdictional claims in published maps and institutional affiliations.

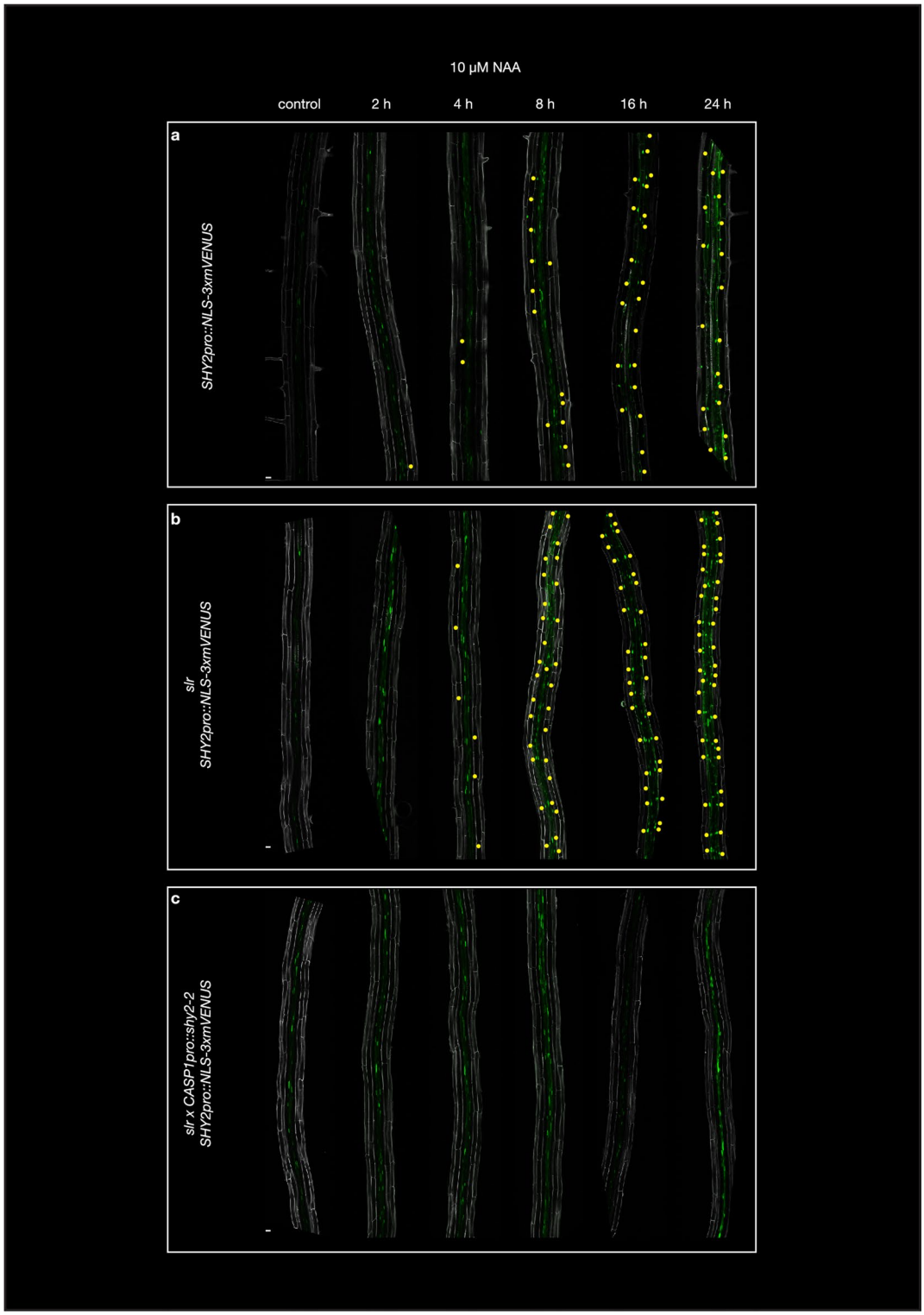

Extended Data Fig. 1 | *SHY2pro::NLS-3xmVENUS* dynamics in Col-0 (a), *slr-1* (b) and *CASP1pro::shy2-2/slr-1* treated with NAA. a. Maximum image projections of roots expressing *SHY2pro::NLS-3xmVENUS* in Col-0 **(a)**, *slr-1* **(b)** and *CASP1pro::shy2-2/slr-1* **(c)** after 2, 4, 8, 16 and 24 hours of NAA treatment. Yellow dots indicate *SHY2pro::NLS-3xmVENUS* signal in the endodermis. The images in are representatives of each experiment repeated 3 times. Scale bar in (**a**) = 50 µm.

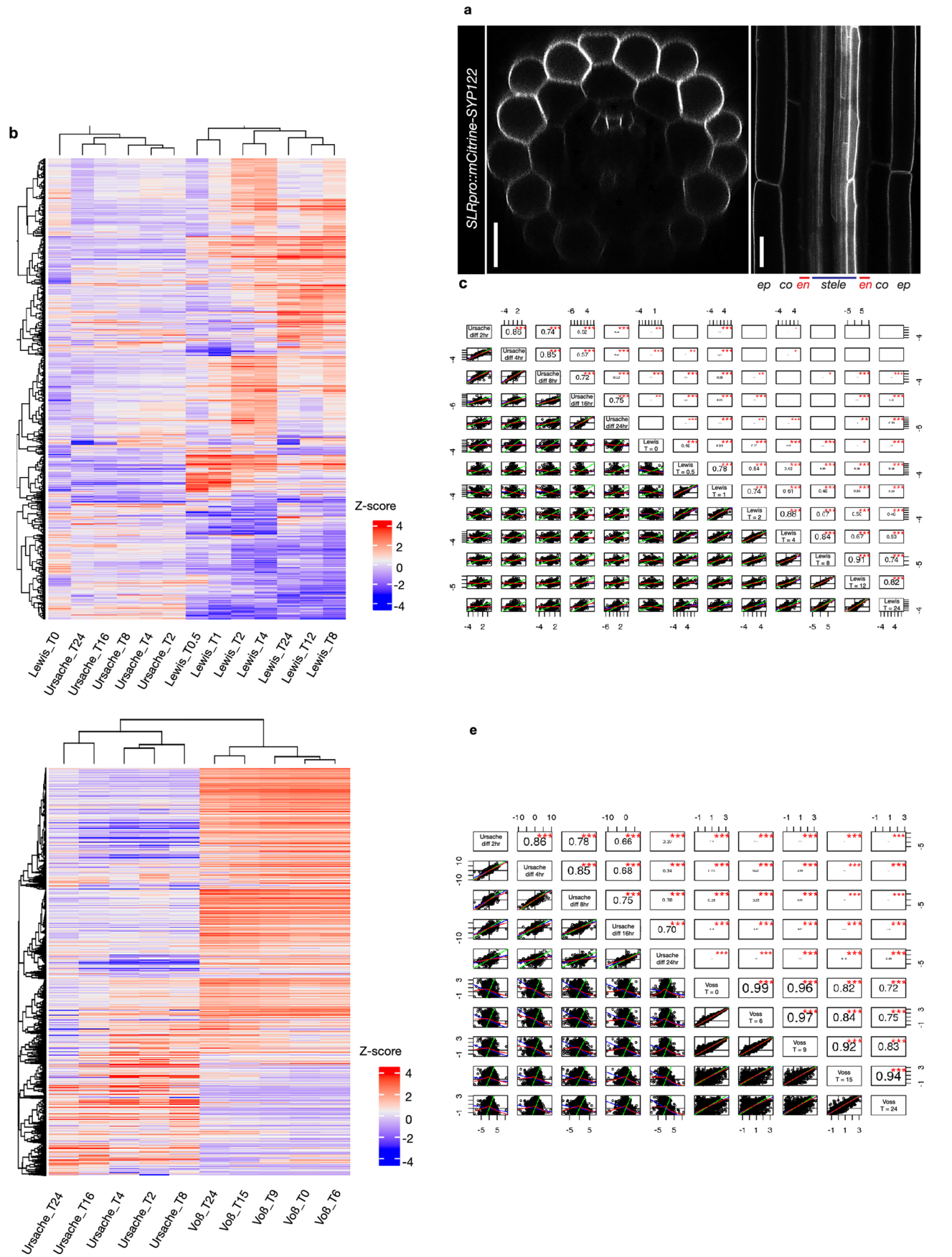

Extended Data Fig. 2 | See next page for caption.

Extended Data Fig. 2 | Differentiated endodermal cells have a distinct transcriptional response to auxin. a, Confocal images of a root expressing *SLRpro::CITRINE:SYP122* confirming that *SLR* is expressed in the epidermis, cortex, pericycle and weakly in the stele, but not in the endodermis (indicated by asterisks). The images are representatives of the experiment repeated 3 times. **b** and **c**, Comparison of the current dataset (Ursache) with the data set of Lewis et al.[14]. **b**, Heatmap showing that both datasets cluster separately and do not have significant overlap, which is confirmed by the analysis of correlation between the two data sets (**c**). **d** and **e**, Comparison of the current dataset (Ursache) with the data set of Voß et al.[15]. **d**, Heatmap showing that both datasets cluster separately and do not have significant overlap, which is confirmed by the analysis of correlation between the two data sets (**e**). *p* values in **c** and **e** are derived from a Pearson correlation test, are two-sided t-test values and not corrected for multiple testing. The corresponding cut-points (*/**/***) represent here $p < 0.05$, $p < 0.01$ and $p < 0.001$. The r value measures the correlation between 2 sets of data. The p-value states whether there are enough observations to believe that an observed correlation is not appearing by chance. Scale bar = 25 μm.

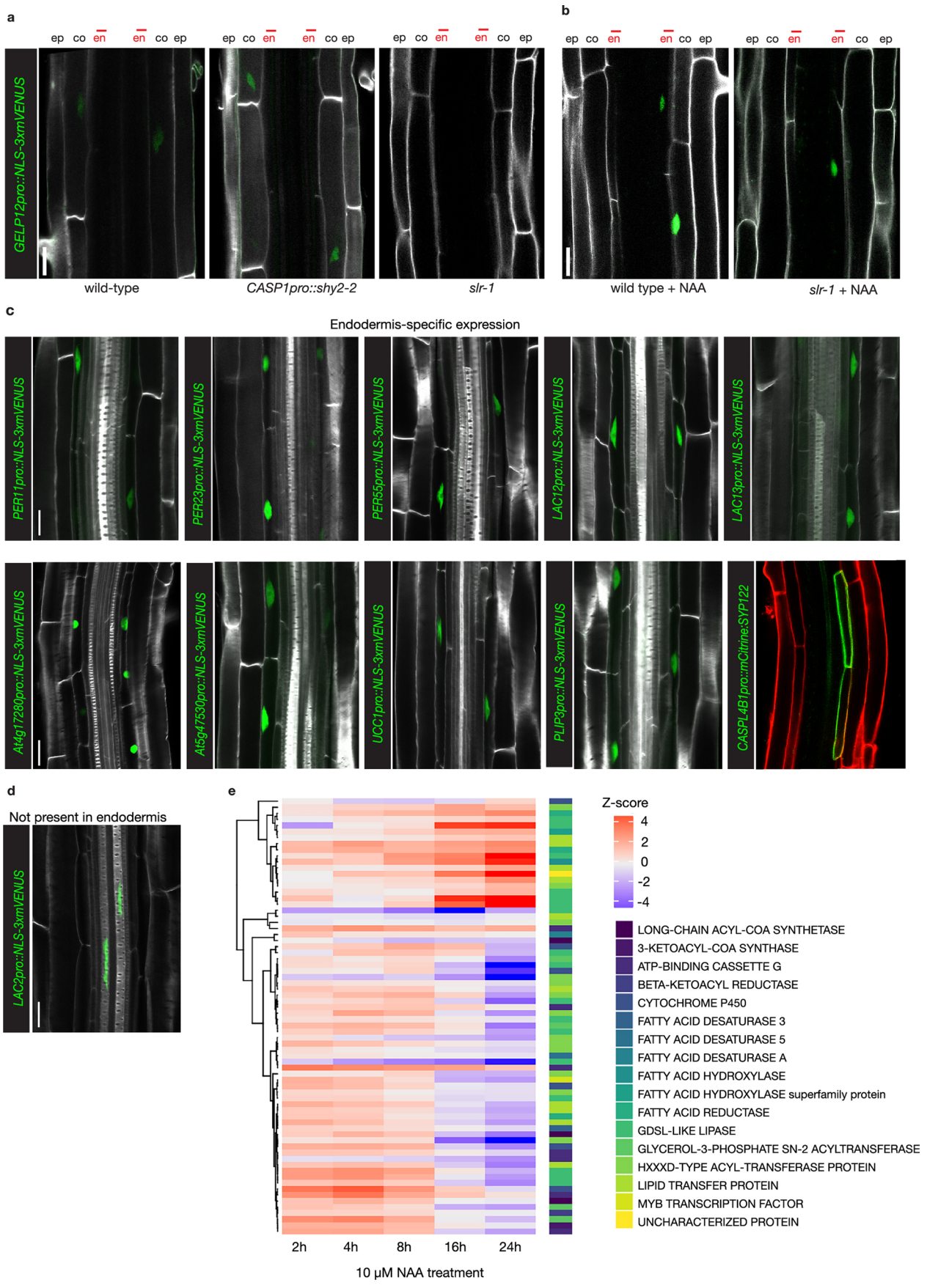

Extended Data Fig. 3 | See next page for caption.

Extended Data Fig. 3 | A high number of differentially regulated genes are expressed in the endodermis. a, Confocal images of *GELP12pro::NLS-3xmVENUS* expression in different genetic backgrounds, showing repression in *slr-1* under control conditions. **b**, Auxin treatment (10 μM NAA, 16hrs) results in induction of *GELP12pro::NLS-3xmVENUS* expression in the endodermis of *slr-1* roots. NLS-3xmVENUS signal is shown in green and CFW staining of cell walls is shown in grey. **c**, Confocal images of roots expressing transcriptional markers of candidate genes differentially expressed between *slr-1* and *CASP1pro::shy2-2/slr-1* roots and showing specific expression in the endodermis. **d**, Confocal images showing xylem-specific expression of *LAC2pro::NLS-3xmVENUS*. **e**, Heatmap showing the expression dynamics of suberin-related genes significant differentially expressed. NLS-3xmVENUS signal is shown in green, CFW staining of cell walls in gray and cell wall staining by PI in red. The images in **(a-d)** are representatives of each experiment repeated at least 3 times. Scale bars = 20 μm.

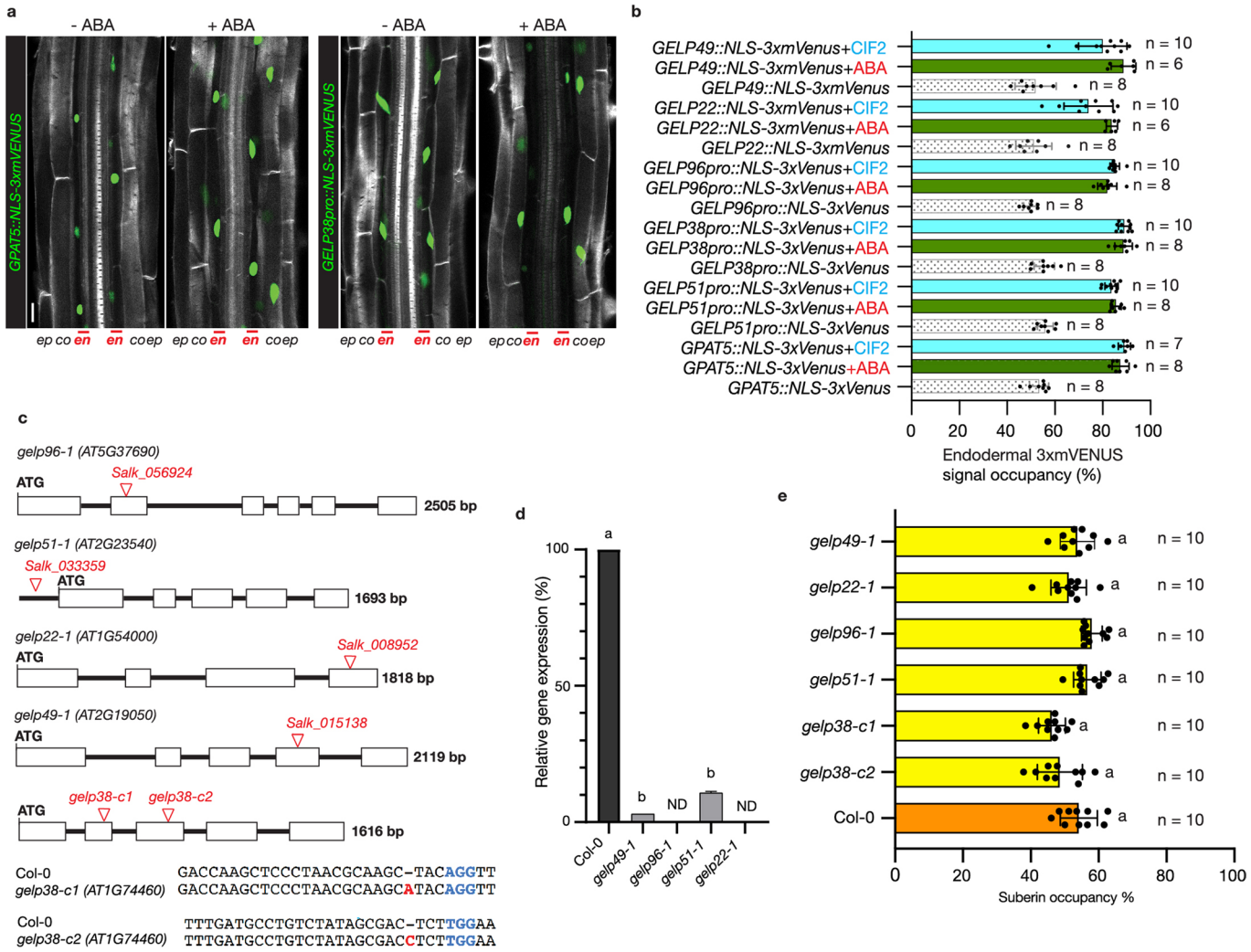

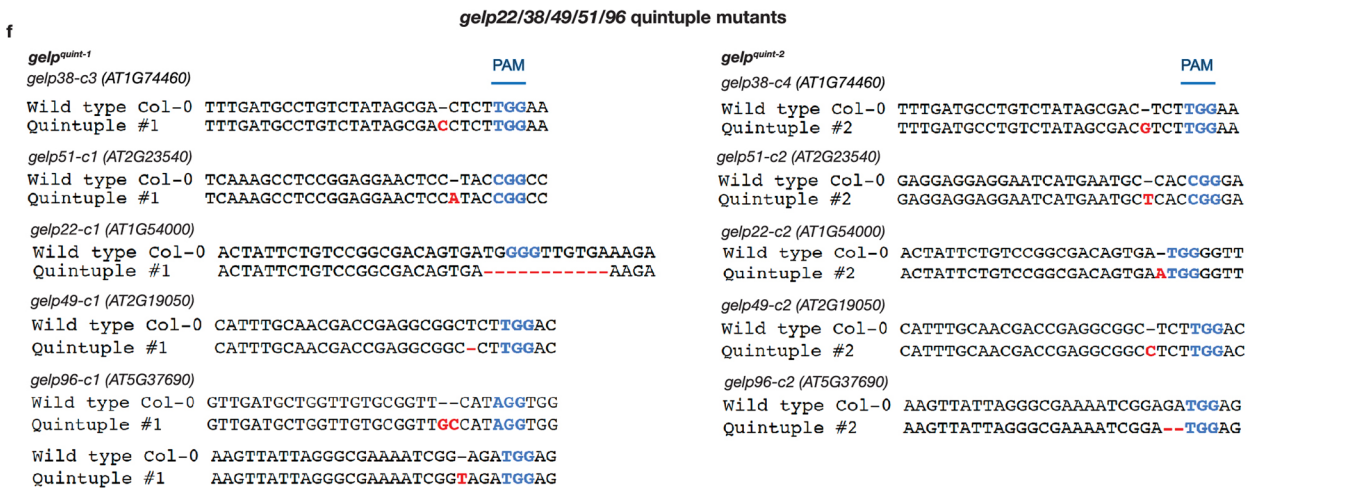

Extended Data Fig. 4 | See next page for caption.

Extended Data Fig. 4 | Expression of suberin biosynthesis-related GELPs is induced by ABA and CIF2 treatment. a, Confocal images showing effect of ABA treatment (1 μM, 24hr) on the expression domain of *GPAT5pro::NLS-3xmVENUS* and *GELP38pro::NLS-3xmVENUS* in Arabidopsis roots. The images are representatives of the experiment repeated 3 times. **b**, Quantification of the effect of ABA (1 μM, 24hr) and CIF2 peptide (500 nM, 24h) treatment on the expression of suberin biosynthesis-related GELPs identified as being repressed by auxin treatment. **c**, Schematic representation of the different single mutants of the suberin biosynthesis-related GELPs used in this study. **d**, qPCR results showing the relative gene expression in Col-0 control (100%) and T-DNA insertion lines of the suberin synthesis-related GELPs used in this study. The results are based on three biological replicates. The *p* value versus the Col-0 control for *gelp49-1* is <0.000001 and for *gelp51-1* is < 0.000001. ND, not detected. **e**, Quantification of suberin occupancy in the endodermis of the single mutants of the suberin biosynthesis-related GELPs using FY staining (n = 10 biologically independent samples). The *p* value versus the Col-0 control for *gelp38-c1* is 0.1269, for *gelp38-c2* is 0.2616, for *gelp51-1* is > 0.9999, for *gelp96-1* is 0.9385, for *gelp22-1* is > 0.9999 and for *gelp49-1* is > 0.9999. Different letters in **(d)** and **(e)** ($p < 0.05$) indicate statistically significant differences between means by ANOVA and two-sided t-test analysis. **f**, Schematic representation of the mutations in the $gelp^{quint\text{-}1}$ and $gelp^{quint\text{-}2}$ mutants. The mutations are indicated in red and the PAM sites in blue. Error bars in **(b)**, **(d)** and **(e)** are SD. Scale bar in (**a**) = 25 μm.

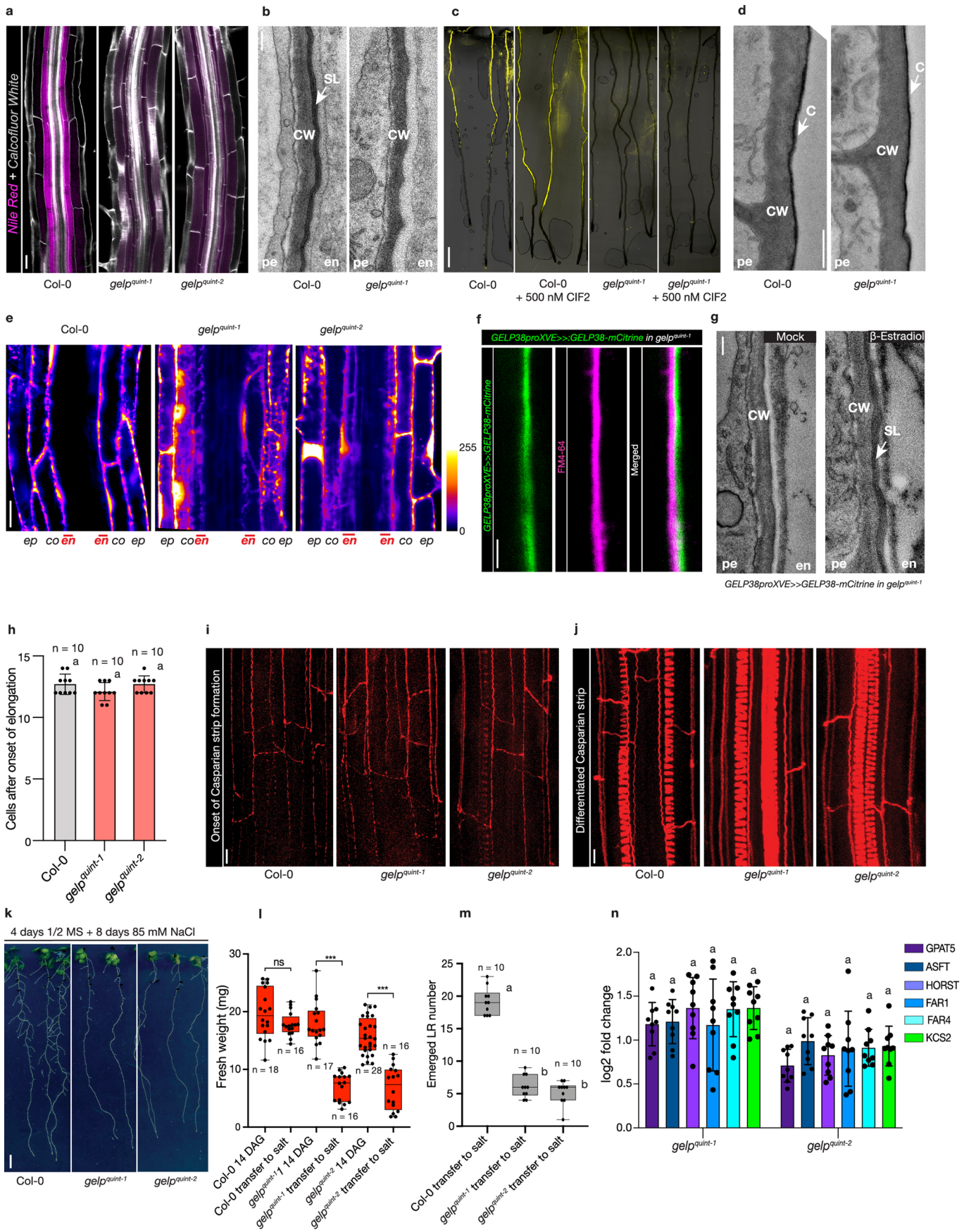

Extended Data Fig. 5 | See next page for caption.

Extended Data Fig. 5 | Extended characterization of the phenotype of *gelp*^{quint} mutants. a, Nile Red staining of wild-type and *gelp*$^{quint-1}$ and *gelp*$^{quint-2}$ roots confirms the absence of suberin in the mutants. **b**, TEM micrographs of high-pressure frozen roots of wild-type and *gelp*$^{quint-1}$ showing the absence of suberin lamella in the mutant. A region without lateral root primordia has been chosen to highlight the absence of suberin lamella. **c**, FY staining of CIF2 peptide treated Col-0 and *gelp*$^{quint-1}$ seedlings showing absence of CIF2-mediated suberin deposition in *gelp*$^{quint-1}$. **d**, TEM micrograph of high-pressure frozen roots of wild-type and *gelp*$^{quint-1}$ showing that the lateral root cap cuticle is not affected in the *gelp*$^{quint-1}$ mutant. **e**, Fluorescein di-acetate (FDA) uptake assay in wild-type roots showing a suberin mediated block of uptake at the level of the endodermis. **f**, Confocal image of a root expressing *GELP38-XVEpro::GELP38- mCITRINE* (green) in *gelp*$^{quint-1}$ after β-Estradiol treatment (5 μM) stained with FM4-64 dye. **g**, TEM micrographs of roots of *gelp*$^{quint-1}$ and the complementation by *GELP38-XVEpro::GELP38- mCITRINE* showing the complete recovery of endodermis suberin lamella. The images in **(a-g)** are representatives of each experiment repeated at least 3 times. **h**, Counting of PI-stained cells as a proxy for Casparian strip barrier in the roots of wild-type and *gelp*$^{quint-1}$ and *gelp*$^{quint-2}$ seedlings. All individual data points are plotted. No statistically significant difference was detected in using ANOVA and Bonferroni-adjusted paired two-sided t-test. The *p* value versus the Col-0 control for *gelp*$^{quint-1}$ is 0.1680 and for *gelp*$^{quint-2}$ is > 0.9999. **i-j**, Basic Fuchsin staining of the Casparian strip in early and differentiated endodermal cells of wild-type and *gelp*$^{quint-1}$ and *gelp*$^{quint-2}$ roots. **k**, Salt stress assay showing that *gelp*$^{quint-1}$ and *gelp*$^{quint-2}$ mutant seedlings are more sensitive to mild salt stress (85 mM NaCl) compared to wild-type. The images in **(i-k)** are representatives of each experiment repeated at least 3 times. **l**, Quantification of the effect of prolonged salt stress on the fresh weight of wild-type and *gelp*$^{quint-1}$ and *gelp*$^{quint-2}$ seedlings. All individual data points are plotted. The *p* value versus the Col-0 control for Col-0 transferred to salt is 0.7857, for *gelp*^{quint1} versus *gelp*^{quint1} transferred to salt is < 0.000001 and for *gelp*$^{quint-2}$ versus *gelp*$^{quint-2}$ transferred to salt is < 0.000001. **m**, Quantification of emerged lateral roots in wild-type and *gelp*$^{quint-1}$ and *gelp*$^{quint-2}$ mutants after 8 days of exposure to salt. All individual data points are plotted (n = 10). **n**, Quantification of the expression of known suberin biosynthesis-related genes in *gelp*$^{quint-1}$ and *gelp*$^{quint-2}$ mutants. Results are presented as fold-change compared to their expression levels in Col-0 (n = 9). No statistically significant difference was detected in using ANOVA and Bonferroni-adjusted paired two-sided t-test. For GPAT5, the *p* value versus Col-0 for *gelp*$^{quint-1}$ is > 0.9999 and for *gelp*$^{quint-2}$ is 0.4546, for ASFT the *p* values are > 0.9999 and > 0.9999; for HORST the *p* values are 0.1122 and > 0.9999; for FAR1 the *p* values are > 0.9999 and > 0.9999; for FAR4 the *p* values are 0.1467 and > 0.9999; for KSC2 the *p* values are 0.1136 and > 0.9999 correspondingly. Different letters in **(m)** ($p < 0.001$) and asterisks in **(l)** ($p < 0.001$) indicate statistically significant differences between means by ANOVA and two-sided t-test analysis. ns, not significant. For the boxplots in **(l)** and **(m)** the center depicts the median while the lower and upper box limits depict the 25th and 75th percentile respectively. Whiskers represent minima and maxima. Closed dots depict individual samples. Data in **(h)** and **(n)** are presented as mean +/- SD. Scale bars for **(a), (d), (e), (f), (g), (h-j)** = 25 μm. Scale bars for **(b)** and **(c)** = 1 μm, for **(k)** = 5 mm.

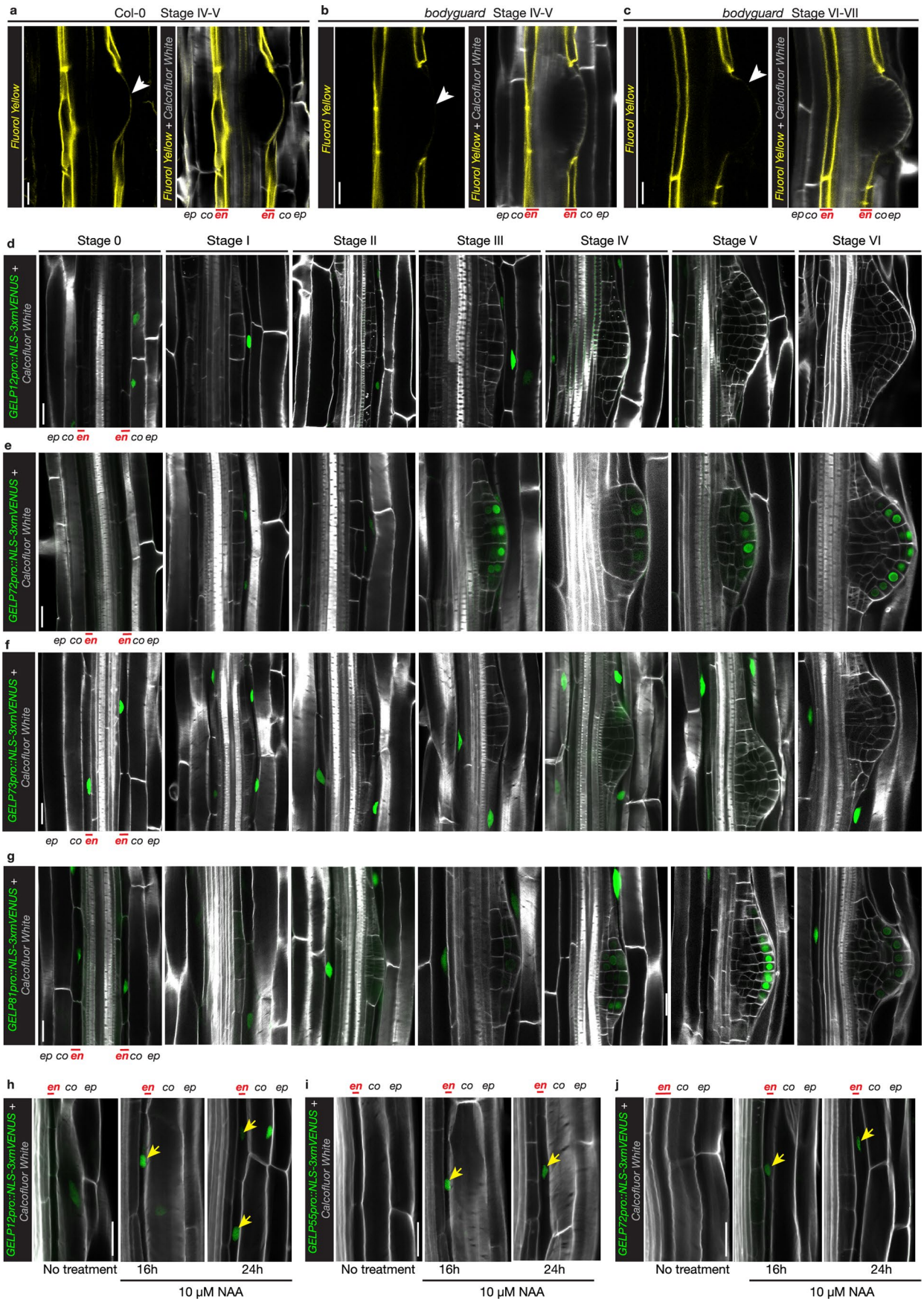

Extended Data Fig. 6 | See next page for caption.

Extended Data Fig. 6 | Auxin-upregulated GELPs show three distinct expression patterns. a, FY staining of a Col-0 root at the site of lateral root emergence highlighting the presence of cuticle (indicated by arrow). **b-c**, FY staining of *bodyguard* mutant root at the site lateral root emergence. The absence of a proper cuticle is highlighted by the gap in FY staining. **d-g**, Confocal images showing the expression patterns of *GELP12* **(d)**, *GELP72* **(e)**, *GELP73* (**f**) and *GELP81* **(g)** during lateral root emergence. **h-j**, Confocal images showing the expression of *GELP12* **(h)**, *GELP55* **(i)** and *GELP72* **(j)** after 10 μM NAA treatment. NLS-3xmVENUS signal is in green and Calcofluor White staining of cell walls is in gray. The images are representatives of each experiment repeated at least 3 times. Scale bars = 25 μm.

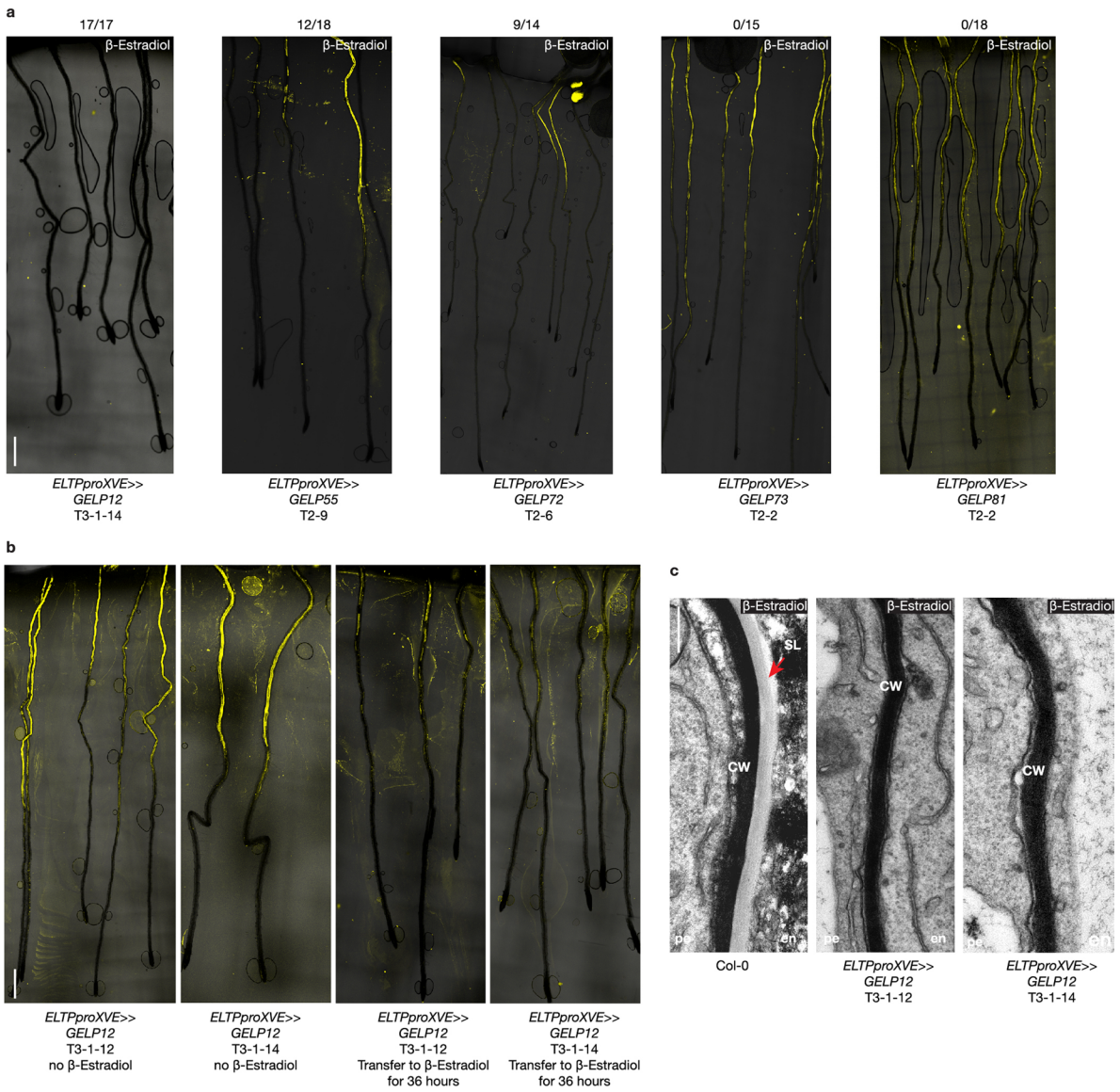

d

Single CRISPR mutants for auxin-upregulated GELPs:

	gRNA1 PAM	gRNA2 PAM
Col-0	AAGCTTACGATGAGCGAAGCC-ATGAGGAGA	GTTTTACAAGAAAGGCACGAT-CCAAGGCGG
gelp12-c1 (AT1G28650)	AAGCTTACGATGAGCGAAGCCCATGAGGAGA	GTTTTACAAGAAAGGCACGATTCCAAGGCGG
Col-0	AAGCTTACGATGAGCGAAGCCATGAGGAGA	GTTTTACAAGAAAGGCACGAT-CCAAGGCGG
gelp12-c2 (AT1G28650)	AAGCTTACGATGA--------CATGAGGAGA	GTTTTACAAGAAAGGCACGATTCCAAGGCGG
Col-0	GGTTGCCGAAATATTGTGGTC-GGAGGGTTA	
gelp55-c1 (AT2G30310)	GGTTGCCGAAATATTGTGGTCCGGAGGGTTA	
Col-0	GGTTGCCGAAATATTGTGGTC-GGAGGGTTA	CAATGTAATTGTAGGCAGC-TTCCGAGGGAT
gelp55-c2 (AT2G30310)	GGTTGCCGAAATATTGTGGTCAGGAGGGTTA	CAATGTAATTGTAGGCAGCTTTCCGAGGGAT
Col-0	TGCTAACGTTAAGCATCCAGTTGCTGGATG	
gelp72-c1(AT3G48460)	TGCTAACGTTAAGCATCCAGT-GCTGGATG	
Col-0	ACAATTACCTAGTCCCTTTTGTCGCGGCTC	
gelp73-c1 (AT3G50400)	ACAATTACCTAGTCCCTTTT-TCGCGGCTC	
Col-0	CCATCTCGTGGAAATCCAACC-GGCCGGTTT	TATGGACGCTCGGAAATTTGT-GGTGGGAAA
gelp73-c2 (AT3G50400)	CCATCTCGTGGAAATCCAACCTGGCCGGTTT	TATGGACGCTCGGAAATTTGTTGGTGGGAAA
Col-0	TCAAAGTAATCCCGGCCATATGGCTGGAAA	
gelp81-c1 (AT4G26790)	TCAAAGTAATCCCGGT--------TGGAAA	
	14bp insertion+334bp deletion	
gelp81-c2 (AT4G26790)	GTTCTGAAGAGCAATTTCCAGCCCAGGCTACTACAAA-334bp deletion-GAATACTACAAAGAATACC	

Extended Data Fig. 7 | See next page for caption.

Extended Data Fig. 7 | Overexpression of three auxin-induced GELPs leads to suberin degradation. a, FY staining on roots of Col-0 treated with b-Estradiol results in normal suberin pattern, whereas inducible endodermis-specific overexpression of *GELP12*, *GELP55* or *GELP72* results in degradation of suberin highlighted by absence of FY signal. The overexpression of GELP73 and GELP81 results in a normal suberin pattern similar to wild-type. **b**, FY staining of *ELTPproXVE>>GELP12* lines germinated on normal 1/2MS medium for 4 days and transferred to the plates supplemented with 5 μM β-estradiol for 36 hours to observe the suberin degradation. **c**, TEM micrographs of *ELTPproXVE>>GELP12* grown on plates with and without β-estradiol to highlight the absence of suberin lamella upon induction of GELP12 expression in endodermis. **d**, Schematic representation of the mutations in the auxin-upregulated single GELP mutants. The mutations are indicated in red and the PAM sites in blue. The images in **(a-c)** are representatives of each experiment repeated at least 3 times. Scale bars in **(a)** and **(b)** = 500 μm. Scale bars in **(c)** = 1 μm.

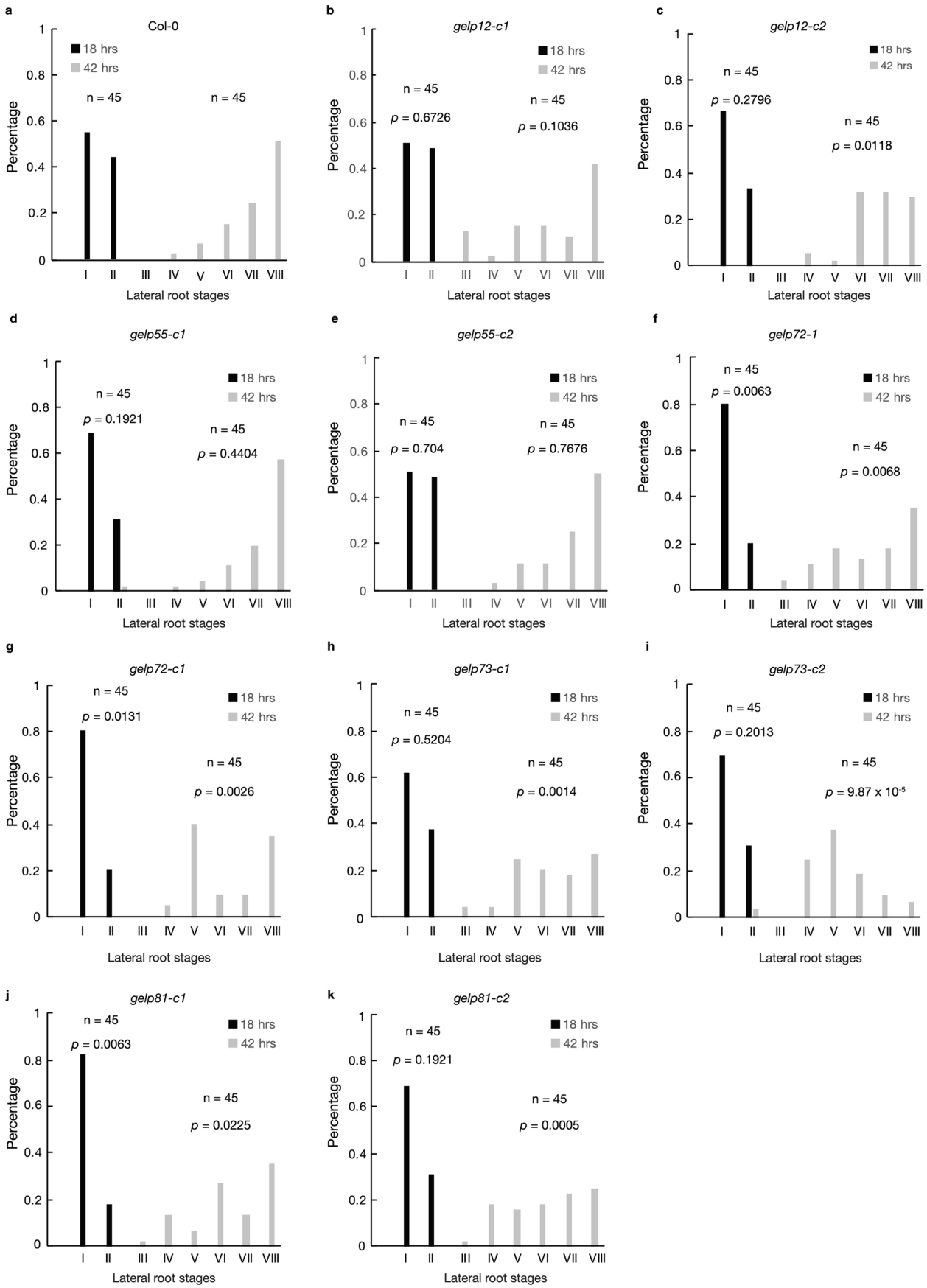

Extended Data Fig. 8 | See next page for caption.

Extended Data Fig. 8 | Some auxin-inducible GELPs facilitate lateral root emergence. a-**k**, Gravistimulation-mediated induction of lateral root formation to functionally characterize the role of auxin-induced *GELPs* during lateral root formation. Staging of lateral root development was performed at 18hr and 42hr after gravistimulation. **a**, Col-0. **b** and **c**, *gelp12-c1* and *gelp12-c2*. **d** and **e**, *gelp55-c1* and *gelp55-c2*. **f** and **g**, *gelp72-1* and *gelp72-c1*. **h** and **i**, *gelp73-c1* and *gelp73-c2*. **j** and **k**, *p* values are indicated. A *p* value below 0.05 indicates a statistically significant difference as determined using a Pearson's χ^2 test. Experiments were repeated three times with a minimal of 15 seedlings per genotype and time point.

nature research

Corresponding author(s): Robertas Ursache, Niko Geldner, Joop Vermeer

Last updated by author(s): Jan 4, 2021

Reporting Summary

Nature Research wishes to improve the reproducibility of the work that we publish. This form provides structure for consistency and transparency in reporting. For further information on Nature Research policies, see our Editorial Policies and the Editorial Policy Checklist.

Statistics

For all statistical analyses, confirm that the following items are present in the figure legend, table legend, main text, or Methods section.

n/a	Confirmed	
☐	☒	The exact sample size (*n*) for each experimental group/condition, given as a discrete number and unit of measurement
☐	☒	A statement on whether measurements were taken from distinct samples or whether the same sample was measured repeatedly
☐	☒	The statistical test(s) used AND whether they are one- or two-sided *Only common tests should be described solely by name; describe more complex techniques in the Methods section.*
☐	☒	A description of all covariates tested
☐	☒	A description of any assumptions or corrections, such as tests of normality and adjustment for multiple comparisons
☐	☒	A full description of the statistical parameters including central tendency (e.g. means) or other basic estimates (e.g. regression coefficient) AND variation (e.g. standard deviation) or associated estimates of uncertainty (e.g. confidence intervals)
☐	☒	For null hypothesis testing, the test statistic (e.g. *F*, *t*, *r*) with confidence intervals, effect sizes, degrees of freedom and *P* value noted *Give P values as exact values whenever suitable.*
☒	☐	For Bayesian analysis, information on the choice of priors and Markov chain Monte Carlo settings
☒	☐	For hierarchical and complex designs, identification of the appropriate level for tests and full reporting of outcomes
☒	☐	Estimates of effect sizes (e.g. Cohen's *d*, Pearson's *r*), indicating how they were calculated

Our web collection on statistics for biologists contains articles on many of the points above.

Software and code

Policy information about availability of computer code

Data collection	Leica-Leica Application Suite X (version 3.1.5.16308 and 3.5.6.21594 to collect images on a Leica SP8 and Leica SP8-MP, respectively. Zeiss-Zen 2.1 SP3 (Black edition) to collect image on a Zeiss LSM880.
Data analysis	Image J (Version 2.0.0-rc-69/1.52p (build: 269a0ad53f) for image analysis Microsoft Excel for Mac version 16.39, Graphpad Prism (Version 9.0.0 (86)) and R (version 3.5.1) for statistical analysis.

For manuscripts utilizing custom algorithms or software that are central to the research but not yet described in published literature, software must be made available to editors and reviewers. We strongly encourage code deposition in a community repository (e.g. GitHub). See the Nature Research guidelines for submitting code & software for further information.

Data

Policy information about availability of data

All manuscripts must include a data availability statement. This statement should provide the following information, where applicable:

- Accession codes, unique identifiers, or web links for publicly available datasets
- A list of figures that have associated raw data
- A description of any restrictions on data availability

All data is available in the Extended Data Figures, Supplemental files and NGS-data is available at GEO. All used plant lines and accession numbers are mentioned in the data availability section. In addition, the data supporting the findings in this study are available from the corresponding author upon reasonable request.

Field-specific reporting

Please select the one below that is the best fit for your research. If you are not sure, read the appropriate sections before making your selection.

☒ Life sciences ☐ Behavioural & social sciences ☐ Ecological, evolutionary & environmental sciences

For a reference copy of the document with all sections, see nature.com/documents/nr-reporting-summary-flat.pdf

Life sciences study design

All studies must disclose on these points even when the disclosure is negative.

Sample size	The determination of sample size was according to in-house protocols that have been established on 10 years of experience in root phenotyping and on the widely-used sample sizes in the root developmental community. Generally, for the comparison of root development (fresh weight, primary root length, lateral root development and histological staining) we aim at at sample size of 15 to 20 roots per genotype per biological replication.
Data exclusions	No data were excluded.
Replication	Each experiment was reproduced at least 3 times, none were found to be non-reproducible. Root bending experiments were performed independently by different researchers yielding similar results.
Randomization	The samples used in this study (plants) in combination with the performed experiments (phenotyping of control and mutant plants) is not subjected to intrinsic bias that would require randomization to overcome this.
Blinding	Experiments were not blinded due to the fact that we need to perform imaging experiments. The phenotypes of the different genotypes used for the RNAseq are very obvious thus blinding id not very effective in that case. The suberin phenotype was also extremely striking and hence blinding would not be very effective.

Reporting for specific materials, systems and methods

We require information from authors about some types of materials, experimental systems and methods used in many studies. Here, indicate whether each material, system or method listed is relevant to your study. If you are not sure if a list item applies to your research, read the appropriate section before selecting a response.

Materials & experimental systems

n/a	Involved in the study
☒	☐ Antibodies
☒	☐ Eukaryotic cell lines
☒	☐ Palaeontology and archaeology
☒	☐ Animals and other organisms
☒	☐ Human research participants
☒	☐ Clinical data
☒	☐ Dual use research of concern

Methods

n/a	Involved in the study
☒	☐ ChIP-seq
☒	☐ Flow cytometry
☒	☐ MRI-based neuroimaging